JOURNAL OF GEOPHYSICAL RESEARCH: ATMOSPHERES, VOL. 118, 5750–5769, doi:10.1002/jgrd.50434, 2013

Validation of ozone data from the Superconducting Submillimeter-Wave Limb-Emission Sounder (SMILES)

Koji Imai,[1] Naohiro Manago,[2] Chihiro Mitsuda,[3] Yoko Naito,[4] Eriko Nishimoto,[4] Takatoshi Sakazaki,[5] Masatomo Fujiwara,[5] Lucien Froidevaux,[6] Thomas von Clarmann,[7] Gabriele P. Stiller,[7] Donal P. Murtagh,[8] Ping-ping Rong,[9] Martin G. Mlynczak,[9] Kaley A. Walker,[10,11] Douglas E. Kinnison,[12] Hideharu Akiyoshi,[13] Tetsu Nakamura,[13,14] Takayuki Miyasaka,[3] Toshiyuki Nishibori,[1] Satoko Mizobuchi,[15] Ken-ichi Kikuchi,[16] Hiroyuki Ozeki,[17] Chikako Takahashi,[3] Hiroo Hayashi,[3] Takuki Sano,[1] Makoto Suzuki,[1] Masahiro Takayanagi,[1] and Masato Shiotani[1,18]

Received 26 September 2012; revised 17 April 2013; accepted 18 April 2013; published 6 June 2013.

[1] The Superconducting Submillimeter-Wave Limb-Emission Sounder (SMILES) onboard the International Space Station provided global measurements of ozone profiles in the middle atmosphere from 12 October 2009 to 21 April 2010. We present validation studies of the SMILES version 2.1 ozone product based on coincidence statistics with satellite observations and outputs of chemistry and transport models (CTMs). Comparisons of the stratospheric ozone with correlative data show agreements that are generally within 10%. In the mesosphere, the agreement is also good and better than 30% even at a high altitude of 73 km, and the SMILES measurements with their local time coverage also capture the diurnal variability very well. The recommended altitude range for scientific use is from 16 to 73 km. We note that the SMILES ozone values for altitude above 26 km are smaller than some of the correlative satellite datasets; conversely the SMILES values in the lower stratosphere tend to be larger than correlative data, particularly in the tropics, with less than 8% difference below ~24 km. The larger values in the lower stratosphere are probably due to departure of retrieval results between two detection bands at altitudes below 28 km; it is ~3% at 24 km and is increasing rapidly down below.

Citation: Imai, K., et al. (2013), Validation of ozone data from the Superconducting Submillimeter-Wave Limb-Emission Sounder (SMILES), *J. Geophys. Res. Atmos.*, *118*, 5750–5769, doi:10.1002/jgrd.50434.

1. Introduction

[2] Ozone is one of the most important constituents throughout the Earth's atmosphere. It plays a major role in controlling the Earth's radiation budget and consequently shielding us from solar ultraviolet rays, so, it is crucial to make accurate measurements of its global distribution. It is important also to monitor its temporal variation, as we are now in the beginning of the slow recovery stage of the ozone layer after serious losses in the Antarctic ozone hole [*WMO*, 2007].

[3] To demonstrate the high sensitivity of the 4-K cooled submillimeter limb sounder in the environment of outer space, and to monitor the global distribution of middle-atmosphere trace gases, the Superconducting Submillimeter-Wave Limb-Emission Sounder (SMILES) was developed and

[1]Institute of Space and Astronautical Science, Japan Aerospace Exploration Agency, Sagamihara, Japan.
[2]Center for Environmental Remote Sensing, Chiba University, Chiba, Japan.
[3]Fujitsu FIP Corporation, Tokyo, Japan.
[4]Faculty of Science, Kyoto University, Kyoto, Japan.
[5]Graduate School of Environmental Science, Hokkaido University, Sapporo, Japan.
[6]Jet Propulsion Laboratory, California Institute of Technology, Pasadena, California, USA.
[7]Karlsruhe Institute of Technology, Institute für Meteorologie und Klimaforschung, Karlsruhe, Germany.
[8]Department of Radio and Space Sciences, Chalmers University of Technology, Göteborg, Sweden.
Corresponding author: K. Imai, Institute of Space and Astronautical Science, Japan Aerospace Exploration Agency, Sagamihara, Japan. (imai.koji@jaxa.jp)

2169-897X/13/10.1002/jgrd.50434

[9]Center for Atmospheric Sciences, Hampton University, Hampton, Virginia, USA.
[10]Department of Physics, University of Toronto, Toronto, Canada.
[11]Department of Chemistry, University of Waterloo, Waterloo, Canada.
[12]Atmospheric Chemistry Division, National Center for Atmospheric Research, Boulder, USA.
[13]Center for Global Environmental Research, National Institute for Environmental Studies, Tsukuba, Japan.
[14]Arctic Environment Research Center, National Institute of Polar Research, Tachikawa, Japan.
[15]Systems Engineering Consultants Co., LTD, Tokyo, Japan.
[16]Applied Electromagnetic Research Institute, National Institute of Information and Communications Technology, Koganei, Japan.
[17]Department of Environmental Science, Faculty of Science, Toho University, Funabashi, Japan.
[18]Research Institute for Sustainable Humanosphere, Kyoto University, Uji, Japan.

deployed on the Japanese Experiment Module (JEM) on the International Space Station (ISS). This was done through cooperation between the Japan Aerospace Exploration Agency (JAXA) and the National Institute of Information and Communications Technology (NICT). SMILES conducted high sensitivity limb soundings for the middle atmosphere from 12 October 2009 to 21 April 2010 (see the overview by *Kikuchi et al*. [2010a]). Taking advantage of the non-sun-synchronous orbit of the ISS, SMILES also measured the diurnal variation of minor atmospheric constituents such as O_3, ClO, HO_2 and BrO. The SMILES high sensitivity measurements at varying local times (LT) are expected to provide not only further insights into atmospheric chemistry but also reestimation of long-term trends based on fixed LT measurements; the variations of the stratospheric and mesospheric ozone are described in *Sakazaki et al*. [2013] and *Smith et al.* [2013], respectively.

[4] The SMILES Level 2 (L2) data processing system [*Mitsuda et al*., 2011; *Takahashi et al*., 2010, 2011] retrieves vertical profiles of minor atmospheric constituents from the calibrated radiance observations (Level 1 data). SMILES version 2.1 (hereafter v2.1) L2 products were released for public use in March 2012. In this study, using other space borne observation data and the output from chemistry and transport models as supplementary data, we validate the altitude range from 16 to 79 km and establish characteristics of the SMILES ozone product. We have done similar comparisons of the SMILES ozone data with worldwide ozonesonde measurements in the mid- and lower stratosphere, and found that the agreement is basically good. However, as we noticed that there may be a possible problem in ozonesonde measurements particularly in the equatorial lower stratosphere, which were inferred from the SMILES data, we will present the comparison result in a separate paper.

[5] In general, satellite data have good coverage in both space and time. Thus, many coincidence events are expected, which will give robust conclusions for the accuracy (or statistical error) of the SMILES products. In this validation study we use data from the following five satellite instruments: the Microwave Limb Sounder (MLS) on the Earth Observing System (EOS) Aura satellite [*Waters et al*., 2006], the Michelson Interferometer for Passive Atmospheric Sounding (MIPAS) on the Envisat satellite [*Fischer et al*., 2008], the Sub-Millimetre Radiometer (SMR) on the Odin satellite [*Murtagh et al*., 2002], the Sounding of the Atmosphere using Broadband Emission Radiometry (SABER) instrument on the Thermosphere Ionosphere Mesosphere Energetics and Dynamics (TIMED) satellite [*Russell et al*., 1999], and the Atmospheric Chemistry Experiment-Fourier Transform Spectrometer (ACE-FTS) on the SCISAT-1 satellite [*Bernath et al*., 2005].

[6] In addition to these satellite data, we use model output from two chemistry-climate models (CCMs): the Whole Atmosphere Community Climate Model Version 4 (WACCM4) driven with specified dynamical fields (SD-WACCM) [*Kunz et al*., 2011, and references therein] and the MIROC3.2-CTM developed from the chemical module of the Center for Climate System Research/National Institute for Environmental Studies (CCSR/NIES) CCM [*Akiyoshi et al*., 2009, 2010]. The CCM results used in this study are from simulations that are "nudged" with operational meteorological fields; hereafter, the nudged CCMs are simply referred to as chemistry and transport models (CTMs). The background meteorological conditions are constrained by temperature and wind fields taken from the NASA Global Modeling and Assimilation Office (GMAO) Goddard Earth Observing System Model, Version 5 [GEOS-5; *Rienecker et al*., 2008], and consequently, the distributions of minor species are dynamically and photo-chemically controlled within the model in a consistent manner. Therefore, the resulting distributions of the minor constituents from the CTMs can be considered as a good reference dataset.

[7] Recent inter-satellite validation studies of ozone [e.g., *Verronen et al*., 2005; *Cortesi et al*., 2007; *Steck et al*., 2007; *Froidevaux et al*., 2008; *Jégou et al*., 2008; *Dupuy et al*., 2009; *Rong et al*., 2009; *Mieruch et al*., 2012; *Smith* et al., 2013] showed that agreement is mostly within 20%, 10% and 20% in the lower, mid- and upper stratosphere, respectively. The agreement becomes worse as altitude increases: mostly within 40% (20%) for daytime (nighttime) in the lower mesosphere and this difference widens to more than 60% (50%) in the upper mesosphere where ozone is very low (< 0.2 ppmv) during both day and night (see also section 3 about the characteristics for each data source used in the study). Also, there are differences in ozone profiles among CCMs [e.g., *SPARC CCMVal*, 2010, Figure 6.17; *Oman et al*., 2010]. *Eyring et al*. [2007, 2010] and *Austin et al*. [2010a, 2010b] showed that there were substantial quantitative differences in the recovery time of Antarctic springtime column ozone among projections from the CCMs. The difference is partly due to the difference in the evolution of Cl_y amount in the Antarctic lower stratosphere [*Eyring et al*., 2007; *Oman et al*., 2010; *SPARC CCMVal*, 2010, Figure 5.11]. A simulation for past atmospheric conditions using CTMs or nudged CCMs is planned for the next round of the chemistry-climate model validation activity. Inter-comparison between CTM results and satellite measurements is expected to provide more reasonable constraints on CCMs and at the same time to impose higher requirements on observations.

[8] The remainder of this paper is organized as follows: the SMILES ozone measurements and its L2 data description are presented in section 2; a brief description of the data sources used in this study is given in section 3, and coincidence criteria with the satellite data and the analysis method are covered in section 4. In section 5, we present the comparisons between the SMILES ozone and other data sources. Since the diurnal variation is larger in the mesosphere than in the stratosphere, we show the comparison separately for these two regions. A summary of the work is presented in section 6.

2. SMILES Ozone Measurement and Product

2.1. Overview

[9] After deployment on the JEM, SMILES measured the Earth's limb from 12 October 2009 to 21 April 2010; failure of a critical component in the submillimeter local oscillator then terminated SMILES observations. To carry out high-sensitivity measurements for submillimeter limb-emission sounding, SMILES carried a superconductor-insulator-superconductor (SIS) junction device, which was cooled down to 4 K using

a two stage Stirling cycle cooler and a Joule-Thomson cooler [*Narasaki et al*., 2004]. The frequency spectra were obtained by two sets of acousto-optical spectrometers (AOSes) [*Ozeki et al*., 2000], each of which has 1728 spectrometer channels and covers a bandwidth of approximately 1.2 GHz. Their frequency resolution is approximately 1.8 MHz (FWHM), and the channel separation is typically 0.8 MHz. The instrumental performance in orbit is described by *Ochiai et al*. [2010]. Since the antenna beam is deflected 45° left from the direction of orbital motion, SMILES nominally covered latitudes from 38°S to 65°N on each orbit within a 93 min period. The ISS is not in a sun-synchronous orbit and its orbital plane rotates every ~60 days, so SMILES covered all local times within ~30 days. The antenna was scanned in elevation at a period of 53 s, and the total number of scans per day was about 1600.

[10] SMILES has three specified detection bands within the submillimeter-wave region: 624.32–625.52 GHz (Band A), 625.12–626.32 GHz (Band B), and 649.12–650.32 GHz (Band C). Since the instrument contained two sets of AOS [*Ozeki et al*., 2000], two of the three detection bands (Bands A, B, and C) were measured simultaneously, and the spectrometer in Band A could be switched to the different AOS units such as Bands A (1) + B (2) and Bands C (1) + A (2) (a number in parentheses is the AOS unit number); this situation is described in detail in *Kikuchi et al*. [2010a, 2010b]. For the ozone retrieval, the measurements of Bands A and B are used, since the brightest ozone emission line in the SMILES measurement bands is the line at 625.371242 GHz, which is located in Bands A and B. Although the possibility of the low-altitude ozone retrieval using ozone emission slope in Band C is discussed by *Takahashi et al*. [2011], this approach was not applied to the present study. SMILES started operation using a fixed combination of the three bands over a period of days, then, daily cyclic observations were performed in the last 2 months or so [*Kikuchi et al*., 2010a].

2.2. Data Description

[11] In this study, we use the SMILES v2.1 L2 product derived from the retrieval system developed by *Takahashi et al*. [2010, 2011], and further improved by *Mitsuda et al*. [2011]. The retrieval algorithm is based on the Optima Estimation Method (OEM) applied for atmospheric sounding [*Rodgers*, 1976, 1990, 2000]. The most probable solution can be derived from statistical combination of a priori knowledge of a state vector $\boldsymbol{x}$ and the information on the measurement. The state vector represents the vertical profiles of target species concentrations, atmospheric temperature, and pointing offset. The a priori knowledge is represented by the expected state $\boldsymbol{x_a}$ and its covariance matrix $\boldsymbol{S_a}$. The diagonal elements of $\boldsymbol{S_a}$ is assumed to be the monthly averaged daytime or nighttime profiles of MLS ozone v2.2 [*Froidevaux et al*., 2008] in each 10° latitude bin over the 3 year period, 2005–2007, and their standard deviations are set as the a priori error. Temperature a priori is GEOS-5 data (6 h interval) [*Rienecker et al*., 2008] and its error is set to be 2 K. We use a modification of the Gauss-Newton method called the Levenberg-Marquardt method [*Levenberg* 1944; *Marquardt* 1963]. The retrieved state vector $\boldsymbol{x_{i+1}}$ at the iterative step $i+1$ is calculated as

$$x_{i+1} = x_i + \left(K_{x_i}^T S_y^{-1} K_{x_i} + S_a^{-1} + \gamma D\right)^{-1} \cdot \left\{K_{x_i}^T S_y^{-1}[y - F(x_i, b)] + S_a^{-1}(x_a - x_i)\right\}. \quad (1)$$

where, the matrix $\boldsymbol{K_{xi}}$ is a weighting function for each of the retrieval parameters evaluated at $\boldsymbol{x_i}$, $\boldsymbol{y}$ is a measurement vector which denotes the calibrated brightness temperature observed by the SMILES, $\boldsymbol{S_y}$ is the covariance matrix of $\boldsymbol{y}$, γ is a Levenberg-Marquardt parameter which is initially set to 100, $\boldsymbol{D}$ is a scaling matrix that is usually assumed to be $\boldsymbol{S_a}^{-1}$, and $\boldsymbol{F}$ is a forward model including both atmospheric radiative transfer and instrument characteristics. The $\boldsymbol{x_a}$ normally corresponds to the initial guess $\boldsymbol{x_0}$.

[12] In this product (in versions above 2.0), we incorporated the latest Level 1B version 007 radiance data, which includes a correction for receiver gain nonlinearity (SIS mixer, amplifiers, and AOS) [*Ochiai et al*., 2012]. This correction reduces the temperature bias in the upper stratosphere, and consequently the bias in other parameters. The air broadening parameters from HITRAN 2008 [*Rothman et al*., 2009] have been applied for ozone instead of JPL Spectral Line Catalogue [*Pickett et al*., 1992], since the air broadening parameter gave better agreements for the tangent height. In addition, we abandoned temperature retrieval above 40 km and referred to the MLS temperature product while applying the tidal components from the latest results of the Global Scale Wave Model (GSWM) [*Zhang et al*., 2010a, 2010b] (GSWM09); the daily-mean is obtained as the average of ascending and descending node data from MLS, while the diurnal variation is reproduced with the diurnal plus semidiurnal tidal components from GSWM09 data, and the sum of the daily-mean and the diurnal variation is used as the reference temperature for the retrieval.

[13] Characteristics of retrieval results are mainly presented by an averaging kernel matrix $\boldsymbol{A}$, which is the sensitivity of the retrieved state to the true state, and a retrieval covariance matrix $\boldsymbol{S}$, whose diagonal elements show the square of the retrieval precision. These are defined as follows:

$$A = \left(K_x^T S_y^{-1} K_x + S_a^{-1}\right)^{-1} K_x^T S_y^{-1} K_x, \quad (2)$$

$$S = \left(K_x^T S_y^{-1} K_x + S_a^{-1}\right)^{-1}. \quad (3)$$

[14] In the nonlinear case, these matrices are calculated by using the results of the final iteration process. The retrieval precision is defined as the square root of the diagonal elements of $\boldsymbol{S}$. Equation (3) means that, if target species have enough information, retrieval precision depends almost on the $\boldsymbol{S_y}$.

[15] The error budgets of the retrieval algorithm are calibration of Level 1 data, smoothing error, retrieval noise, and forward model parameter errors such as insufficient information on the profiles of non-retrieved parameters, approximations of the instrument functions, incorrect input parameters, and approximations of the fast algorithm [*Takahashi et al*., 2011], in which the uncertainties of nonlinearity correction and pressure broadening parameters are main causes of systematic error for the SMILES ozone retrieval.

[16] The SMILES L2 data for a 24 h period from midnight to midnight universal time are stored in HDF-EOS version 5

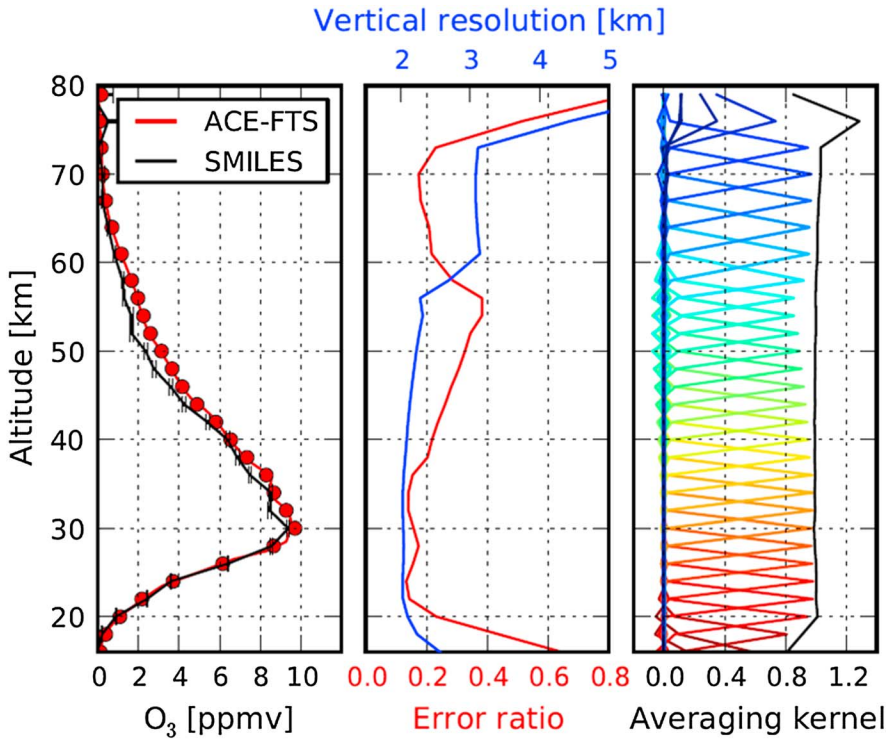

Figure 1. (left) Example of coincident SMILES and ACE-FTS measurements, (middle) the error ratio and vertical resolution, and (right) the averaging kernels. In Figure 1(left), the solid black line and its error bars are a SMILES ozone profile and retrieval precision at 0.07°N and 4.17°E at 15:40:53, 12 October, while the solid red line is a coincident ACE-FTS profile at 0.98°N and 6.94°E at 17:18:06 and the red circles are values convolved with the SMILES ozone averaging kernels. In Figure 1(middle), the red line is the error ratio with corresponding scale shown under the lower axis. The blue line is vertical resolution with corresponding scale shown above the upper axis. In Figure 1(right), colored solid lines show the corresponding vertical averaging kernels as a function of the retrieval level. The solid black line shows the integrated area under each of the colored curves.

files (see also JEM/SMILES L2 Products Guide for v2.1, 2012). The data are now open to the public (see http://darts.jaxa.jp/iss/smiles). The SMILES ozone product provides ozone concentration as volume mixing ratio with the "retrieval precision" [*Rodgers*, 2000; *Takahashi et al*., 2010, 2011] at each SMILES altitude level and with related data screening flags for each profile. The nominal retrieved altitude range is from 8 to 85 km. The vertical grid step of the ozone product is 2 km in the altitude range 8–58 km and 3 km in the altitude range 58–85 km. The "theoretical vertical resolution" is derived from the full width at half maximum (FWHM) of the averaging kernels, which is typically less than ~2.3 km in the altitude range 18–56 km, close to ~3 km from 56 to 61 km and almost constant in the altitude range 61–73 km. We refer to the error ratio (S/S_a) as that of the retrieval precision (S) divided by an a priori error (S_a). Figure 1 shows an example of a single SMILES ozone profile with the retrieval precision, the theoretical vertical resolution, error ratio, and averaging kernels.

[17] The retrieval precision stored in the data file is set as a negative value when the error ratio is larger than 0.5, which means that the estimated precision is larger than 50% of the a priori error. As described in *Takahashi et al*. [2010, 2011], the accuracy of the retrieved ozone profiles is worse at low altitudes because of the uncertainty in the water vapor continuum emission and scattering by clouds. Also the precision becomes worse with decreasing ozone density at high altitudes. The error ratio for ozone typically becomes large below 20 km and above 73 km and exceeds 0.5 below 16 km and above 76 km. In addition, the precision of the SMILES ozone product for the single-scan data is expected to be worse than 10% below 14 km [*Takahashi et al*., 2010, 2011]. Therefore, in this study we consider the altitude range from 16 to 79 km for the validation.

[18] The screening flags include information on the convergence status, the validity of the observation altitude range, and the field-of-view interference with the sun, the moon, and the ISS solar paddle, and are stored in the "status field" as a bit sequence. To assure the validity of the data, in this study we only use the non-flagged profiles with positive retrieval precision. An example of the data screening fields is given in Table 1. A total of 191,854 ozone profiles is available during the SMILES observation period from 12

Table 1. SMILES V2.1 Ozone Data Guidelines

Field	Values to Use	Meaning
Status	= 0	All screening flags for each profile are stored in the status field.
Precision	≥ 0	Negative if the estimated precision is larger than 50% of a priori error.

Table 2. Number of Available Profiles

Band	AOS Unit #	#	%
A	1	38,152	64
	2	74,937	70
B	2	78,765	59
Total		191,854	64

October 2009 to 21 April 2010. This is about 64% of all SMILES profiles including the flagged ones. Among 36% of the remaining profiles, 10% is due to the field-of-view interference caused by the ISS solar paddle, and the remaining 26% is due to the non-convergence in the retrieval system. The total number of available profiles for each combination of bands and spectrometers is listed in Table 2.

[19] As mentioned earlier, SMILES has two detection bands (Bands A and B) and two spectrometers (AOS units 1 and 2) for Band A for ozone measurement. We have noticed some differences in the SMILES measurement characteristics for the different combinations. Figure 2 shows statistical results for the relative differences between the two detection bands and the two spectrometers for Band A. Since SMILES could not simultaneously provide measurements with the combination of the same band or spectrometer such as Band A (1) + A (2) or A (1) + B (1), the results were calculated from the relative differences between SMILES and MLS. As we could not see any trend in the difference between SMILES and MLS, it would appear reasonable to use the MLS data as a reference. However, note that the upper limit of MLS measurements is about 76 km altitude, which is lower than those of SMILES. We performed similar statistics on the SD-WACCM coincident profiles, and we found almost the same result.

[20] Figure 2 shows that the difference between the two bands is within 1% for the altitude range 28–64 km and increases at altitudes below 28 km, reaching about 9% at 20 km. The difference between the two spectrometers is within 3% for the altitude range 20–67 km. As we do not know which band or which spectrometer is better, and the larger number of coincident measurements also increases the stability of the statistics, we used all the available SMILES ozone profiles for our comparison.

3. Data Sources for the Comparison Studies

[21] In the following subsections, we describe briefly the data sources used in this study and the number of profiles coincident with SMILES profiles; the definition of the coincidence criteria is described in detail in section 4. The characteristics for each data set are summarized in Table 3.

3.1. Aura/MLS

[22] The MLS instrument detects thermal emission lines from millimeter to submillimeter wavelengths (between 118 GHz and 2.5 THz) by scanning the Earth's atmospheric limb in a direction ahead of the Aura satellite [*Waters et al.*, 2006]. Since Aura is in a sun-synchronous near-polar orbit with equatorial crossings at about 1:43/13:43 LT [*Schoeberl et al.*, 2006], the measurements are performed during daytime and nighttime. The latitudinal coverage is between 82°S and 82°N. The 240 limb scans per orbit provide almost 3500 profiles per day. This good coverage in both space and time means that there are as many as 35,437 MLS coincident profiles in the whole SMILES observation period. A description of the MLS retrieval approach is given by *Livesey et al.* [2006]. We use the MLS ozone product version 2.2 retrieved from emission lines centered at 235.71 GHz [*Froidevaux et al.*, 2008], which is characterized as follow: the vertical resolution is 2.7–3 km from the upper troposphere to the mid-mesosphere, and the horizontal resolution is mostly between 200 and 300 km. The MLS uncertainty estimates in the stratosphere are often of the order of 5%, with values closer to 10% (and occasionally 20%) at the lowest stratospheric altitudes, where small positive biases can be found. There is no latitudinal dependence from comparisons with other satellite instruments, as well as from aircraft lidar data along the MLS track.

3.2. Envisat/MIPAS

[23] MIPAS is a mid-infrared limb emission spectrometer on the Envisat research satellite [*Fischer et al.*, 2008]. It observes in the wavelength range from 4.15 to 14.6 μm. Envisat is in a sun-synchronous orbit with equatorial crossings around 10:00/22:00 LT. The latitudinal coverage is nominally between 80°S and 80°N. For the reduced-spectral/improved-spatial resolution mode since 2005, it produces 96 limb-scans per orbit in both day and nighttime. Thus, with about 14 orbits a day, a total of about 1300 profiles per day is obtained. There are 15,922 matched profiles in the whole SMILES observation period. We use MIPAS data retrieved through the MIPAS Level 2 research processor developed

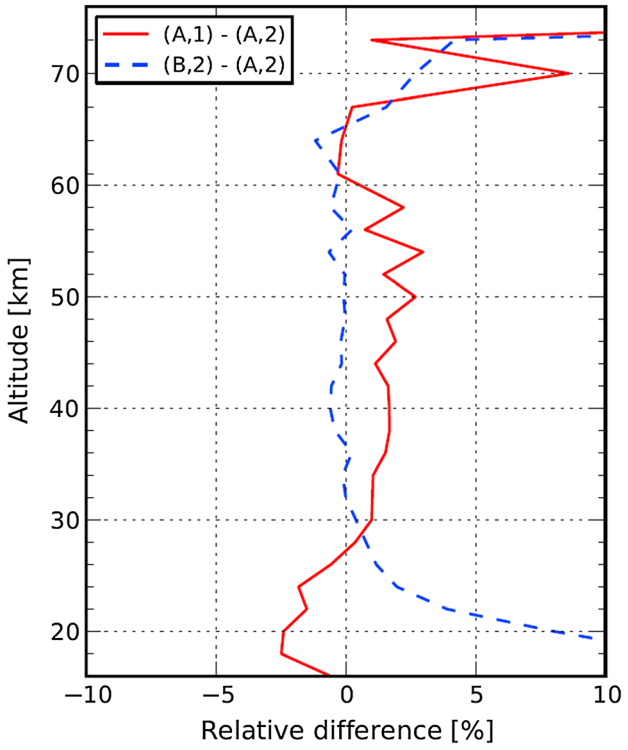

Figure 2. Relative differences between the two bands and the two spectrometers for SMILES. The dashed blue line is the difference between Bands A and B, and the solid red line is the difference between the two spectrometers (AOS units 1 and 2). A detailed description of the calculation procedure can be found in the text.

Table 3. Sampling Characteristics and Data Set Information

Instrument and Model	Latitudinal Coverage	Local Time Measurement and Calculation Time Step	Data Density (Per Day and Horizontal Resolutions)	Number of Coincidence Events	Altitude Coordinate
MLS	82°S–82°N	1:43 (ascending) 13:43 (descending)	3,500	35,437	geopotential
MIPAS	80°S–80°N	~10 (descending) ~22 (ascending)	1,300 since 2005	15,922	geometric
SMR	82.5°S–82.5°N	6:30 (ascending) 18:30 (descending)	630–975	3,161	geometric
SABER	52°S–83°N 83°S–52°N	Non-sun synchronous (except for around between 11:00 and 13:00)	1,400	26,365	geometric
ACE-FTS	85°S–85°N	Sunrise and sunset	30	189	geometric
SMILES	38°S–65°N (nominal)	Non-sun synchronous	1,600		geometric
SD-WACCM	90°S–90°N	30 min	1.9° latitude 2.5° longitude		geopotential
MIROC3.2-CTM	90°S–90°N	30 min	2.6° latitude 2.6° longitude		geopotential

and operated at the Karlsruhe Institute of Technology/IMK [*von Clarmann et al*., 2003, 2009]. The original IMK ozone product was validated by *Steck et al*. [2007]. After a failure of the interferometer, the measurement mode was changed toward reduced spectral but improved spatial resolution. The previous ozone product (version V4O_O3_202) has been described and validated by *Stiller et al*. [2012]. The vertical and horizontal resolutions are 2.4–3.5 km in the altitude range 20–50 km, 253–405 km in the altitude range 10–40 km, respectively. The ozone product has a positive bias of up to 0.9 ppmv around 37 km, but no further significant biases is reported. In this study, we use the most recent data version (V5R_O3_220) [*A. Laeng* personal communication].

3.3. Odin/SMR

[24] The SMR onboard the Odin satellite [*Murtagh et al*., 2002] makes time-shared limb measurements of stratomesospheric ozone using several independent bands within the 486–581 GHz frequency range. Odin is in a sun-synchronous orbit with equatorial crossings at 6:30/18:30 LT. The latitudinal coverage between 82.5°S and 82.5°N is nominally produced during 14–15 orbits per observation day based on 45–65 limb-scans per orbit. A total of 3,161 SMR coincident profiles is found over the SMILES observation period. Vertical profiles of ozone and other species are calculated using retrieval algorithms based on the Optimal Estimation Method [*Frisk et al*., 2003; *Murtagh et al*., 2002]. The operational Level 2 data are produced by the Chalmers University of Technology in Göteborg, Sweden. The SMR ozone product is retrieved from two frequency bands centered at 501.8 GHz and 544.6 GHz [*Urban et al*., 2004, 2005]. We use the SMR 501.8 GHz band retrievals of version 2.1 [*Jégou et al*., 2008]. The vertical and horizontal resolutions are ~3 km in the middle stratosphere, and 500 km along the satellite track, respectively. The SMR version 2.1 ozone shows good agreements with Polar Ozone Atmospheric Measurement (POAM III; within -0.3 ± 0.2 ppmv at 10–60 km), the Network for Detection of Atmospheric Composition Change (NDACC; within -0.15 ± 0.3 ppmv at 10–34 km for ozonesonde, at 10–50 km for lidar, at 10–60 for microwave instruments) and large balloon-borne instruments measurements (within -0.7 ± 1 ppmv at 10–31 km), but the SMR ozone maximum peak is lower than that of POAM III ~1–5 km. No latitudinal dependence has been revealed in the comparisons with NDACC.

3.4. TIMED/SABER

[25] SABER onboard TIMED [*Russell et al*., 1999] is an infrared spectrometer measuring limb emission in the spectral range from 1.27 to 16.9 μm, using a 10 channel broadband infrared radiometer. The two bands at 1.27 and 9.6 μm are used for ozone sounding, and we use both of the version 1.07 SABER ozone products [*Mlynczak et al*., 2007; *Rong et al*., 2009]; hereafter, we refer to these as SABER 1.27 and SABER 9.6, respectively. The TIMED satellite is in a non-sun-synchronous or drifting orbit with a mean orbital time of 97 min. Each day the equator crossing time shifts by approximately 12 min. The spatial coverage alternates approximately every 60 days from 52°S–83°N to 83°S–52°N, and consequently, the latitudes of 52°S–52°N can be observed continuously. There are 26,365 coincident profiles, and the large number of changing LT measurements are useful to focus on the diurnal variation in mesospheric ozone (see section 4). However, note that measurement between around 11:00 and 13:00 LT is not possible, and retrieval of ozone at 1.27 μm is limited to daytime and in the altitude range between mesosphere and lower thermosphere [*Mlynczak et al*., 2007]. The SABER vertical resolution is ~2 km for all channels and all altitudes. The sampling distance is ~500 km along the satellite track. According to *Rong et al*. [2009], the SABER 9.6 has a precision of ~1–2% in the stratosphere and ~3–5% in the lower mesosphere. The positive biases in the stratosphere are within ~5–12% in most cases except in the equatorial to middle latitudes in the altitude range 30–50 km, where they reach ~15–17% and exceed the combined systematic error by ~5–6%.

3.5. SCISAT-1/ACE-FTS

[26] The ACE-FTS sounding of the atmosphere is performed using solar occultation in the infrared (2–13 μm) spectral region, which provides latitudinal coverage of approximately 85°S–85°N with the majority of occultations occurring over the Arctic and Antarctic. Although the solar occultation technique gives less frequent observations (up to 30 occultations per day), ACE-FTS provides

"self-calibrating" measurements of atmospheric absorption spectra with a high signal-to-noise ratio and vertical resolution from an orbit inclined at 74°. This provides a significant number of occultation measurements at high latitudes, and a total of 189 ACE-FTS coincident profiles is found over the SMILES observation period. The ACE-FTS measurements and retrieval technique are described in *Bernath* [2006] and *Boone et al*. [2005], respectively. From the 650 km orbit, the instrument field-of-view (1.25 mrad) corresponds to a maximum vertical resolution of 3–4 km [*Boone et al*., 2005]. ACE-FTS version 2.2 ozone update product reports more ozone than most correlative measurements from the upper troposphere to the lower mesosphere [*Dupuy et al*., 2009]; the mean differences range generally between 0% and 10% with a slight but systematic positive bias (typically +5%) at altitude levels from 16 to 44 km. At higher altitudes up to 60 km, the ACE-FTS ozone amounts are significantly larger than those of the comparison instruments by up to 40% (typically 20%). We use the most recent data version 3.0 [e.g., *Waymark et al*., 2011] for comparisons. At altitudes higher than 35 km the new ACE-FTS version 3.0 ozone profiles have volume mixing ratios 5% lower than those from the version 2.2 update [*K. Walker* personal communication].

3.6. SD-WACCM

[27] WACCM4 is a comprehensive numerical model spanning the range of altitude from the Earth's surface to the thermosphere [*Garcia et al*., 2007]. It is based on the framework of the NCAR Community Atmosphere Model, version 4 (CAM4), and includes all of the physical parameterizations of CAM4 and a finite volume dynamical core [*Lin*, 2004] for tracer advection. Recently, a new version of WACCM4 has been constructed to run with specified dynamical (SD) fields [*Lamarque et al*., 2012]. Temperature and wind fields are taken from the GEOS-5 analysis data [*Rienecker et al*., 2008]; the nudging approach is described in *Kunz et al*. [2011]. The horizontal resolution of the model output is listed in Table 3. The SD-WACCM chemical module is based on the 3-D chemistry and transport Model of Ozone and Related Tracers, Version 3 (MOZART-3) [*Kinnison et al*., 2007]. The chemical and physical processes cover species contained within the O_x, NO_x, HO_x, ClO_x, and BrO_x chemical families, along with CH_4 and its degradation products. In addition, 14 primary non-methane hydrocarbons and related oxygenated organic compounds are included [*Emmons et al*., 2010]. This model contains 122 species, 220 gas-phase reactions, 71 photolytic processes, and 17 heterogeneous reactions on multiple aerosol types. Reaction rate coefficients are based on JPL-2006 [*Sander et al*., 2006]. SD-WACCM has been compared with geophysical measurements to study various atmospheric phenomena in the past [e.g., *Randel et al*., 2010; *Hoffmann et al*., 2012; *Sakazaki et al*., 2013].

3.7. MIROC3.2-CTM (NIES)

[28] CCSR/NIES CCM [*Akiyoshi et al*., 2009, 2010] covers the region from the surface to about 80 km altitude, which has been well-reviewed by comparing to various models and geophysical measurements over the past two decades [e.g., *Butchart et al*., 2011; *Strahan et al*., 2011]. MIROC3.2-CTM was developed by incorporating the chemical module of CCSR/NIES CCM into the MIROC3.2 general circulation model (GCM) that was used for the Fourth Assessment Report of the Intergovernmental Panel on Climate Change (IPCC-AR4). Temperature and horizontal winds were nudged toward the GEOS-5 analysis data [*Rienecker et al*., 2008] with the time scale of one day as the meteorological fields are basically similar to SD-WACCM. MIROC3.2-CTM has the same horizontal and vertical resolutions as those in CCSR/NIES CCM (T42 for horizontal and 34 for vertical from the surface to 0.01 hPa; see also Table 3). The CCM uses a new radiation scheme with a higher resolution for the spectral bins (32 bins) than that of CCSR/NIES CCM (18 bins), a semi-Lagrangian scheme for tracer transport, and hybrid sigma-pressure coordinates in the vertical. The chemical species included in the model are O_x, HO_x, NO_x, ClO_x, BrO_x, hydrocarbons for methane oxidation, and heterogeneous reactions for sulfuric acid aerosols, supercooled ternary solution (STS), Nitric Acid Trihydrate (NAT), and ice particles. The CCM contains 61 species (42 for prediction and 19 for photochemical equilibrium), 165 gas-phase reactions, 42 photolytic processes, and 13 heterogeneous reactions on multiple aerosol types. Reaction rate coefficients are based on JPL-2006 [*Sander et al*., 2006]. Both MIROC3.2-CTM and SD-WACCM have been used to study the global pattern of diurnal ozone variations throughout the stratosphere [*Sakazaki et al*., 2013].

4. Validation Methodology

4.1. Coincidence Criteria

[29] We use the satellite data obtained during the SMILES observation period from 12 October 2009 to 21 April 2010. To find the coincident events, we defined the time and location criteria for coincidence to be within ±2 h, ±2° latitude and ±8° longitude. If multiple coincidences for one ozone profile were found, we selected the nearest measurement in space. However, in the measurement mode of Bands A + B, we used both profiles and the comparisons also include the two profiles corresponding to Bands A and B. Numbers of coincident events for each satellite data set are summarized in Table 3. In the case of the CTMs, we extracted the nearest grid data for all the SMILES observation points. Thus, the maximum difference in time and space is half of the calculation time step and the resolution: ±0.25 h, ±0.95° latitude and ±1.25° longitude for SD-WACCM and ±0.25 h, ±1.3° latitude and longitude for MIROC3.2-CTM. Generally there are many coincidence events at higher latitudes, because the SMILES measurement density is higher at these latitudes [*Kikuchi et al*., 2010a, 2010b].

4.2. Calculation Procedures

[30] For comparisons, the altitude coordinate was converted to geometric height by calculating the normal gravity formula based on the geodetic reference system 1980 [*Moritz*, 2000] to match the SMILES data; thus, the altitude shown in this study is expressed in geometric height (see Table 3 for profile information for each data set). The flagged data points were removed from each altitude level. The profiles were linearly interpolated onto the SMILES altitude levels. Since the averaging kernels for ozone are very close to unity and sharply peaked, the comparison results are

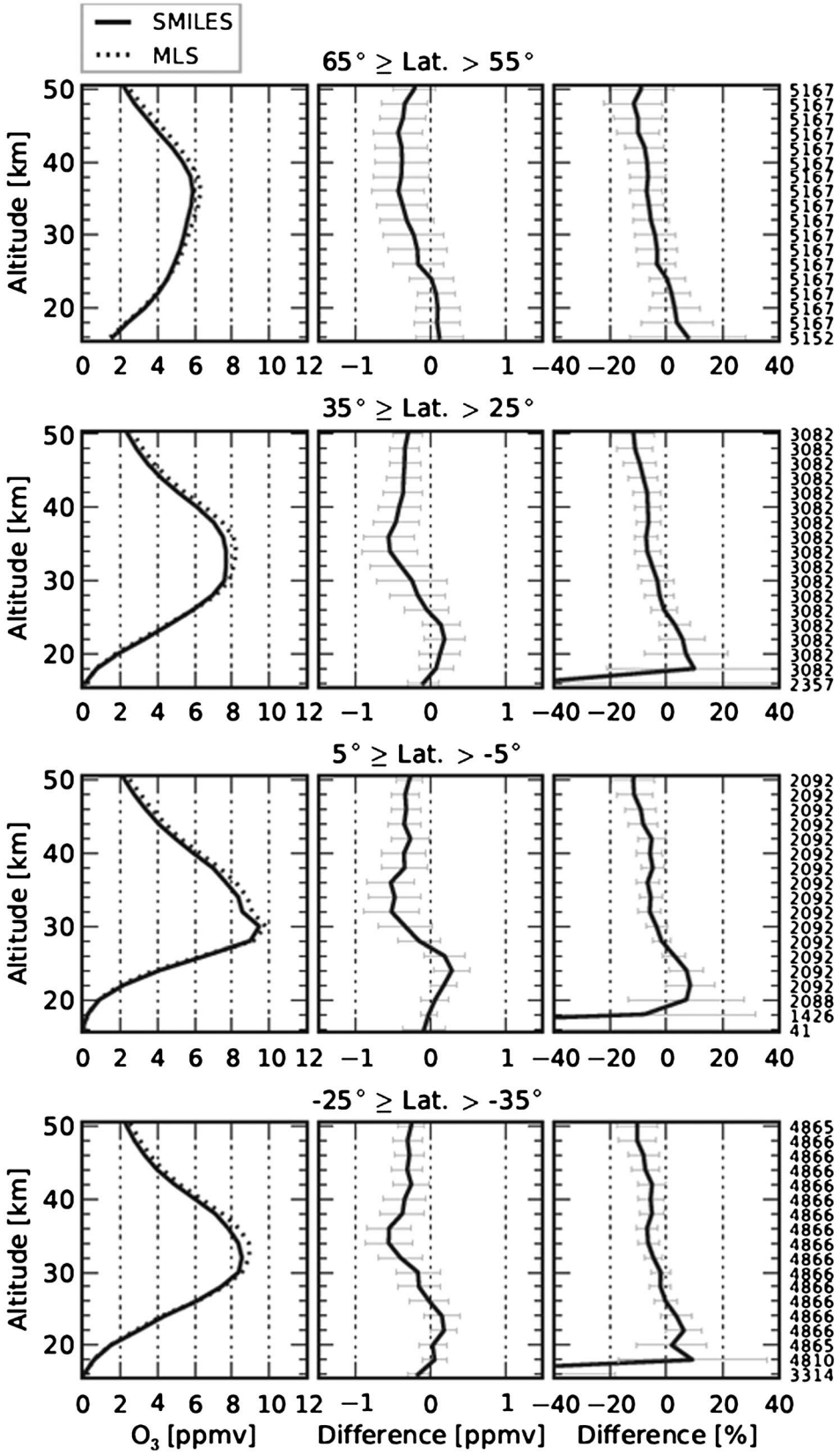

Figure 3. SMILES-MLS coincidences in the stratosphere at four representative latitudes: (from top to bottom) 55°N–65°N, 25°N–35°N, 5°S–5°N, and 35°S–25°S, (left) average ozone values, (middle) average differences (*D*), and (right) average relative differences (*RD*). The solid and dashed lines represent SMILES and MLS profiles, respectively. The error bars represent ±1 standard deviations. The numbers shown on each SMILES altitude level on the right axes are the profile numbers for the statistics.

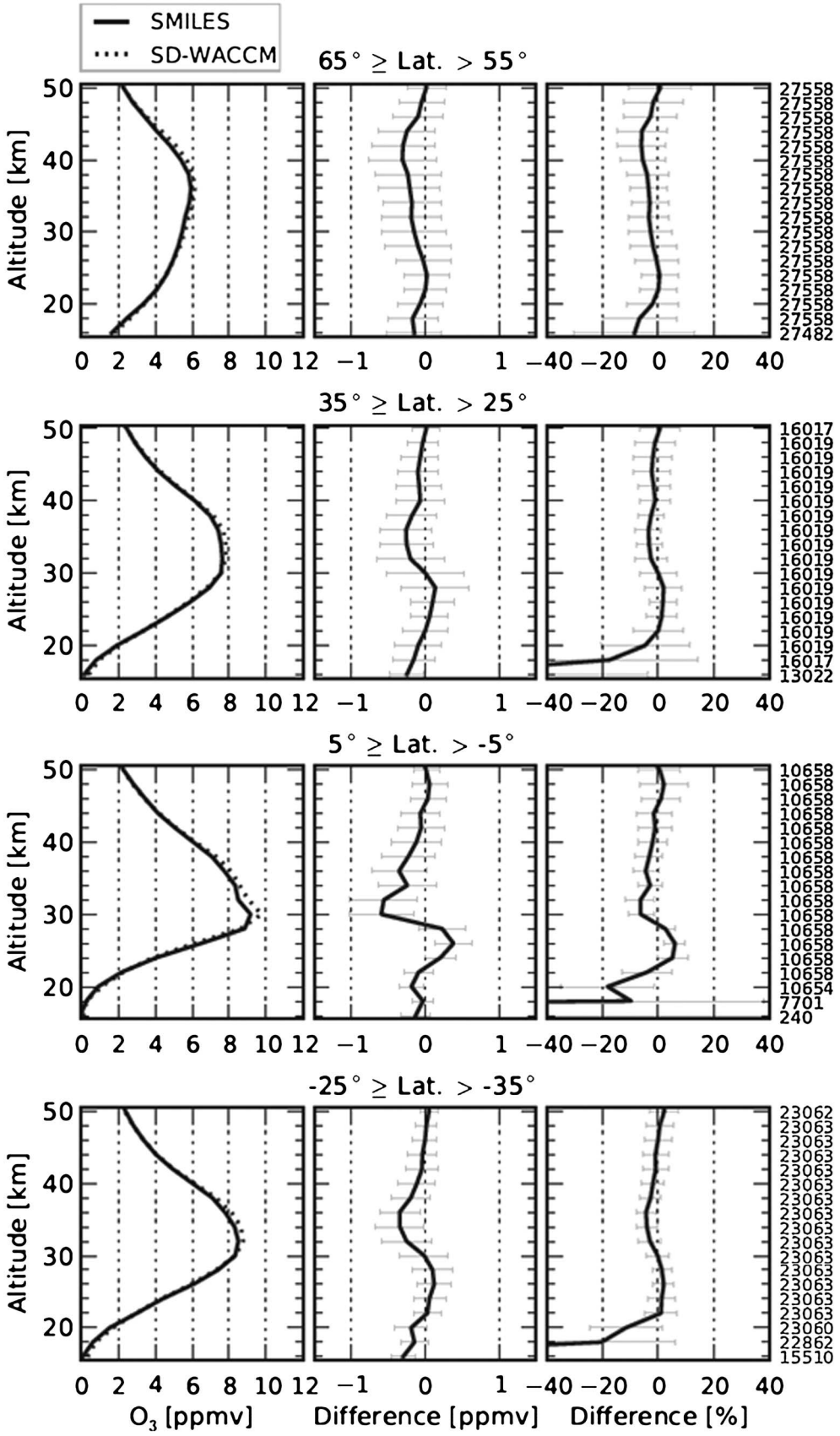

Figure 4. Same as for Figure 3 except for comparisons between SMILES and SD-WACCM.

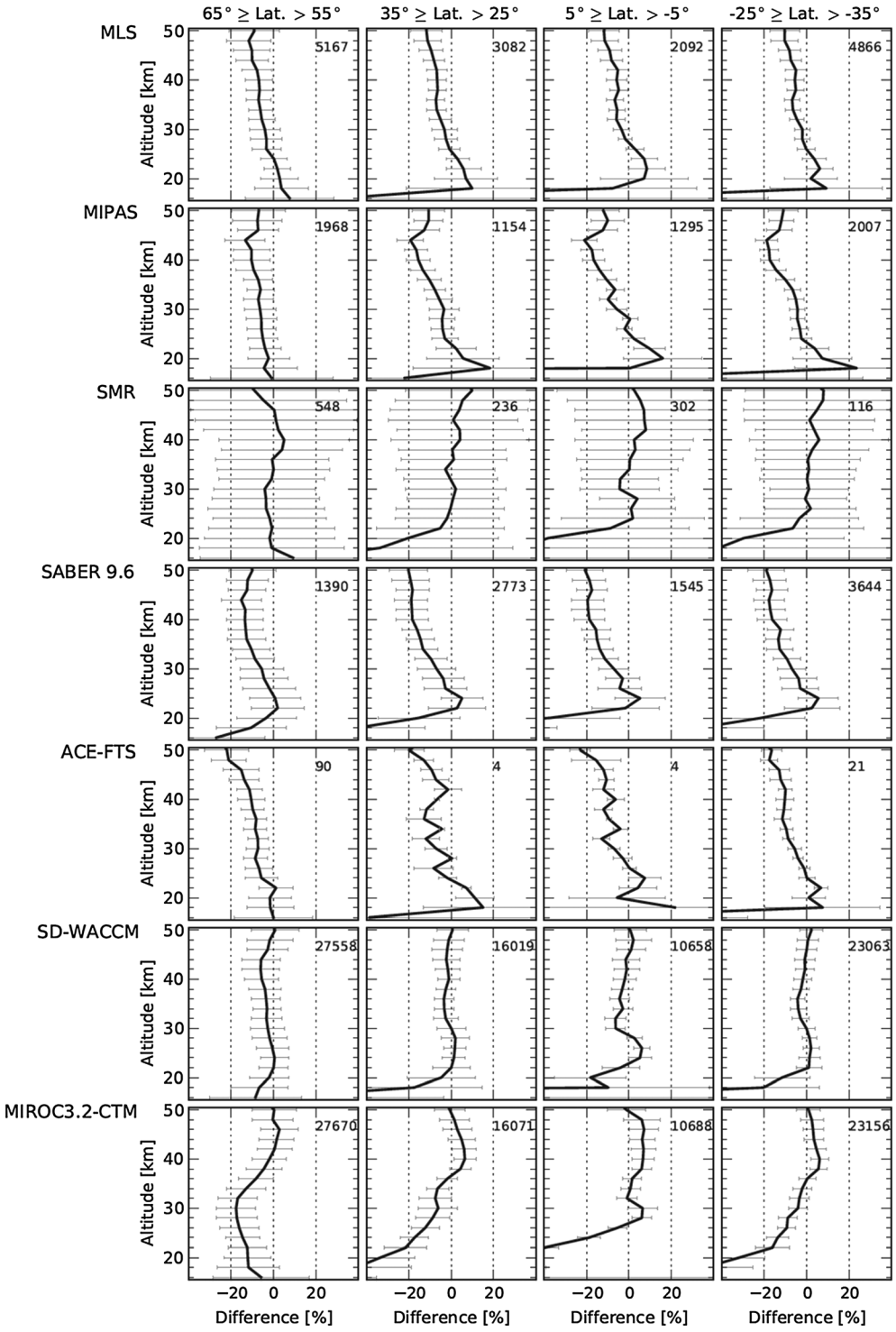

Figure 5. Average relative differences at four representative latitudes: (from top to bottom) comparisons for MLS, MIPAS, SMR, SABER 9.6, ACE-FTS, SD-WACCM, MIROC3.2-CTM, and (from left to right) 55°N–65°N, 25°N–35°N, 5°S–5°N, and 35°S–25°S. Each error bar denotes ±1 standard deviations. The numbers of coincidence events are shown in the upper-right of each panel.

basically similar to those using linear interpolation (see Figure 1). For unrealistically large values occasionally seen in the SABER ozone data [*Rong et al*., 2009], we removed the extreme values (> 100 ppmv) from each altitude level of the interpolated SABER ozone. Then large values are excluded if they exceed three standard deviations (σ) from the median, and we repeat this rejection until the median becomes a constant value.

[31] The average difference (*D*) and average relative difference (*RD*) shown in this study were derived by using reliable data from coincident profiles in the following equations:

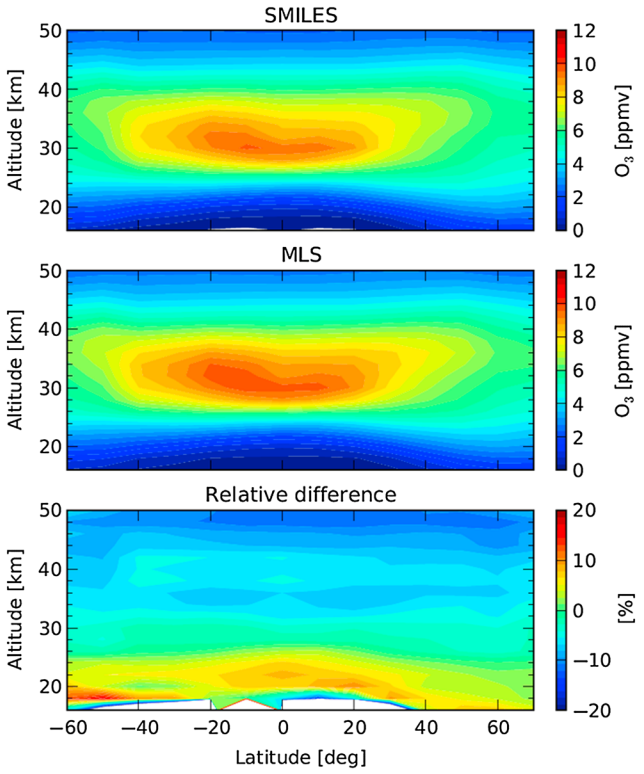

Figure 6. Contour plots of zonally averaged ozone data for SMILES-MLS coincidences: (top) SMILES, (middle) MLS, and (bottom) average relative difference.

$$D = \overline{Q_i - R_i}\ , \tag{4}$$

$$RD = D/\{(\bar{Q}_i + \bar{R}_i)/2\}, \tag{5}$$

where Q_i and R_i are the ith coincidence pair of the SMILES and reference measurements, respectively, expressed as volume mixing ratios and the over-bar denotes the mean.

5. Results

[32] Since the diurnal variation of ozone is larger in the mesosphere than in the stratosphere, we show the comparison results separately, in subsection 5.1 for the stratosphere and in subsection 5.2 for the mesosphere. In fact, using the SMILES data, *Sakazaki et al*. [2013] detected diurnal variation of ozone even in the stratosphere; the peak-to-peak difference may be up to 8% in the middle stratosphere over the course of a day. In this study, we perform the coincidence-based comparisons for the whole day to elucidate the general features. Although even the averaged coincidence measurements are biased at lower latitudes owing to the less-frequent observation (cf. upper-right corner of each panel in Figure 5), the biases are less than ~1% difference in volume mixing ratio in the stratosphere, which is small enough to discuss the accuracy of the SMILES.

5.1. Comparisons in the Stratosphere

[33] Figure 3 shows comparisons of the vertical profiles between SMILES and MLS in four latitude bands. The number of ozone profiles, shown in the right of each right panel in 10° latitude bin, usually decreases for altitudes below 18 km in particular at low latitudes. The decrease at lower altitudes is due to some SMILES ozone profiles with low data quality, which were excluded from the analysis. The ozone profile retrieval in this altitude range was not successful because of the elevated tropopause and resulting low ozone mixing ratios around the tropopause at low latitudes. From the comparisons, we generally see that agreement is reasonable: within 10% in the altitude range 18–46 km and within 12% up to 50 km in the four latitude bands. However, the profiles of the relative differences are weakly inclined, showing that the SMILES ozone has smaller values above ~26 km and larger values below ~26 km. In addition, the difference at equatorial latitudes is slightly larger at ~24 km than in other latitudes. This will be discussed in detail in the comparison results of the latitude-height cross-sections.

[34] Figure 4 is the same as Figure 3 except that the data are from the SD-WACCM coincidences. The agreement is within 7% and better than that of MLS in the altitude range from 18 (22) to 50 km at high (mid and low) latitudes. As a result, the slopes of the relative differences are not as conspicuous as those for MLS. The maximum values of ozone also agree better, although we see a kink around the maxima (25–30 km) particularly at equatorial latitudes. During the SMILES observation period, we found that the ozone distribution in the middle stratosphere at equatorial latitudes was greatly affected by the quasi-biennial oscillation (QBO) and the semi-annual oscillation (SAO). The kink seen at equatorial latitudes may be due to the model's poor representation of vertical motion in association with the QBO and SAO. The relative differences with large negative values below 22 km are not consistent with the results of other comparisons, and we will describe them below.

[35] Figure 5 shows an array of the relative differences for all reference data sets used in this study. Latitude bands for the statistics are similar to those in Figures 3 and 4, so the same figures are presented for MLS and SD-WACCM repeatedly. We see the best agreement with MLS within the satellite data sources and with SD-WACCM out of the two CTM results. This is why we chose to show the MLS and SD-WACCM results in detail in Figures 3 and 4, respectively. In the lower altitudes from 16 (18) to 22 km, the agreement is within 9% (24%) for MLS, MIPAS, ACE-FTS and SD-WACCM at high (mid and low) latitudes; results of MIROC3.2-CTM deviate considerably in this altitude range, except at high latitudes. Note that the comparisons of ACE-FTS at lower latitudes were calculated from significantly fewer coincidences (cf. Table 3 and upper-right corner of each panel in Figure 5). Below 22 km in the lower latitudes, it is difficult to find a consensus among comparisons, because the relative differences vary widely owing to the low data quality of the comparisons as readily seen in the large standard deviations. Some of the SMILES ozone profiles also have low data quality below 18 km, especially in the equatorial latitudes, and these profiles are excluded based on the flag information.

[36] In the altitude range between 22 and 30 km, the inter-satellite and SD-WACCM comparisons agree within 10%, although results of MIROC3.2-CTM still show some biases. In the higher altitude range from 30 to 50 km, the agreement is still generally good for MLS, SMR, and SD-WACCM, but differences reach up to ~20% for MIPAS, SABER 9.6, and ACE-FTS. At this altitude range the

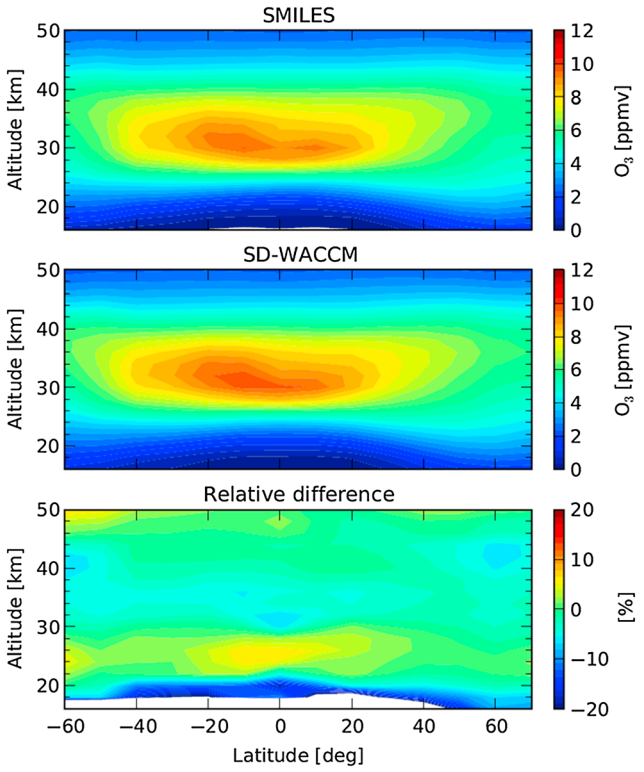

Figure 7. Same as for Figure 6 except for comparisons between SMILES and SD-WACCM.

MIROC3.2-CTM results now show good agreement. There are still other distinct differences seen in individual comparisons, and some of them have been pointed out already in their respective validation studies. Therefore, the following are not necessarily weak points of the SMILES ozone data: the larger negative relative differences around 44 km with respect to MIPAS, especially in the lower latitudes [*Stiller et al.*, 2012; *Laeng* et al., personal communication], the relatively lower precision shown as larger standard deviations in the comparison with SMR [*Jégou et al.*, 2008], the negative relative difference for SABER 9.6 [*Rong et al.*, 2009] and ACE-FTS [*K. Walker* personal communication], and the negative values below 34 km with respect to MIROC3.2-CTM.

[37] Most of the satellite comparison results, except for SMR, show vertical slopes with negative values in the upper stratosphere and positive values in the lower stratosphere. However, two CTM results, if anything, show opposite vertical slopes. Latitudinal characteristics are not so discernible for most of the comparison results, but for MIROC3.2-CTM the difference becomes larger at mid and equatorial latitudes in the lower stratosphere than at high latitudes. These results suggest some shortcomings in the model for this region, such as in the representation of vertical advection, or amounts of water vapor in MIROC3.2-CTM.

[38] Figure 6 shows latitude-height cross-sections of zonal-mean statistics using the SMILES [Figure 6(top)] and MLS [Figure 6(middle)] coincident profiles, respectively. These are figures averaged over almost 6 months centered in the northern winter season. As already seen in Figure 3, the agreement between the two is generally good. Figure 6(bottom) is the average relative difference (*RD*). There is no clear latitudinal dependence above ~28 km, but the SMILES ozone shows slightly larger values with ~8% differences at ~22 km in the equatorial lower stratosphere. This bias will be discussed later with Figure 7. Negative differences increase in the upper stratosphere, reaching ~10% at 50 km.

[39] Figure 7 is the same as Figure 6 except for the comparisons with SD-WACCM. Overall agreement is better than that with MLS. In the mid and upper stratosphere, differences are close to zero except in the upper stratosphere at southern high latitudes. In the lower stratosphere there are also positive differences (~5%) at equatorial latitudes, but they are smaller in SD-WACCM than in MLS. The altitude with maximum differences is located slightly higher for SD-WACCM than for MLS. Also, in this figure we do not see the positive differences in the lower stratosphere at southern high latitude seen in the comparison with MLS (Figure 6). At around the bottom of the stratosphere below ~20 km, the negative differences rapidly become large. We do not know the situation for the real atmosphere, but we may conservatively conclude that the positive bias of the SMILES ozone measurements in the equatorial lower stratosphere, if any, would be of the order of 5%–8%.

[40] To extend our analysis to all the coincident profile pairs for each comparison, we show scatter plots at three representative altitudes (20, 30, and 40 km) in Figure 8. As in Figure 5, we see the best agreement within the satellite data sources with MLS, and with SD-WACCM out of the two CTM results. We note also the very large variability in the SMR measurements. At 20 km, the ozone mixing ratio becomes larger as we move to higher latitudes (red points in the lower left and blue points in the upper right in Figure 8). The latitudinal gradients are reversed at 30 and 40 km and we see the color pattern reverse.

[41] At 20 and 30 km, the SMILES ozone abundances are well correlated with the other data sets, as shown by the tight clusters and a gradient of almost one, although MIROC3.2-CTM shows a large gradient at 30 km. At 40 km, the gradient changes for all cases; for satellite results, the gradients are mostly less than one, and for CTM results, they are greater than one. The standard deviation at all altitudes is comparable to that of the CTMs (SD-WACCM and MIROC3.2-CTM), which means that the uncertainty is smaller than the atmospheric variability for about 6 months.

[42] To summarize the results of the comparison for stratospheric ozone, Figure 9 shows the relative differences averaged for all latitude bands and their standard errors. Owing to the large amount sampling in both space and time of the satellite measurements, the standard errors are less than 1% above 20 km, and the sampling bias is negligible. In the low altitude range from 16 to 22 km, SMILES ozone data show reasonable agreement with MLS, MIPAS, ACE-FTS, and SD-WACCM (particularly good at high latitudes; see Figure 5). Then, from 22 to 30 km, all the satellite data and SD-WACCM agree within ~10%. In the upper stratosphere, we still see good agreement with the two CTMs and with two of the satellite instruments, MLS and SMR. There are however large differences in the upper stratosphere with the observations by MIPAS, SABER 9.6, and ACE-FTS. The differences have negative slopes above ~24 km and widen up to ~20% as the altitude increases. There still remains the uncertainty of tangent altitude

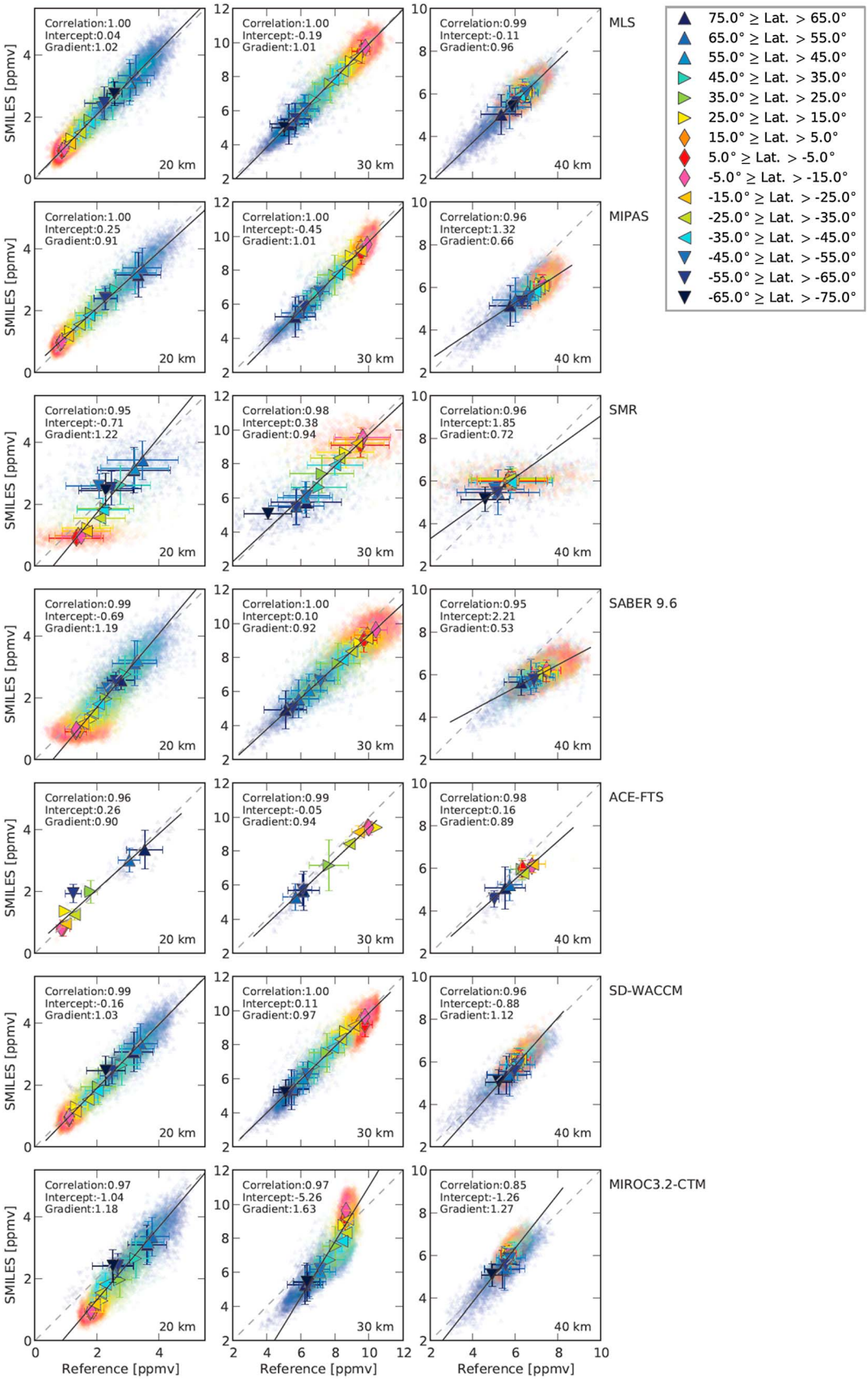
MLS
Correlation:1.00 Intercept:0.04 Gradient:1.02
Correlation:1.00 Intercept:-0.19 Gradient:1.01
Correlation:0.99 Intercept:-0.11 Gradient:0.96
MIPAS
Correlation:1.00 Intercept:0.25 Gradient:0.91
Correlation:1.00 Intercept:-0.45 Gradient:1.01
Correlation:0.96 Intercept:1.32 Gradient:0.66
SMR
Correlation:0.95 Intercept:-0.71 Gradient:1.22
Correlation:0.98 Intercept:0.38 Gradient:0.94
Correlation:0.96 Intercept:1.85 Gradient:0.72
SABER 9.6
Correlation:0.99 Intercept:-0.69 Gradient:1.19
Correlation:1.00 Intercept:0.10 Gradient:0.92
Correlation:0.95 Intercept:2.21 Gradient:0.53
ACE-FTS
Correlation:0.96 Intercept:0.26 Gradient:0.90
Correlation:0.99 Intercept:-0.05 Gradient:0.94
Correlation:0.98 Intercept:0.16 Gradient:0.89
SD-WACCM
Correlation:0.99 Intercept:-0.16 Gradient:1.03
Correlation:1.00 Intercept:0.11 Gradient:0.97
Correlation:0.96 Intercept:-0.88 Gradient:1.12
MIROC3.2-CTM
Correlation:0.97 Intercept:-1.04 Gradient:1.18
Correlation:0.97 Intercept:-5.26 Gradient:1.63
Correlation:0.85 Intercept:-1.26 Gradient:1.27
20 km
30 km
40 km
SMILES [ppmv]
Reference [ppmv]
75.0° ≥ Lat. > 65.0°
65.0° ≥ Lat. > 55.0°
55.0° ≥ Lat. > 45.0°
45.0° ≥ Lat. > 35.0°
35.0° ≥ Lat. > 25.0°
25.0° ≥ Lat. > 15.0°
15.0° ≥ Lat. > 5.0°
5.0° ≥ Lat. > -5.0°
-5.0° ≥ Lat. > -15.0°
-15.0° ≥ Lat. > -25.0°
-25.0° ≥ Lat. > -35.0°
-35.0° ≥ Lat. > -45.0°
-45.0° ≥ Lat. > -55.0°
-55.0° ≥ Lat. > -65.0°
-65.0° ≥ Lat. > -75.0°

Figure 8.

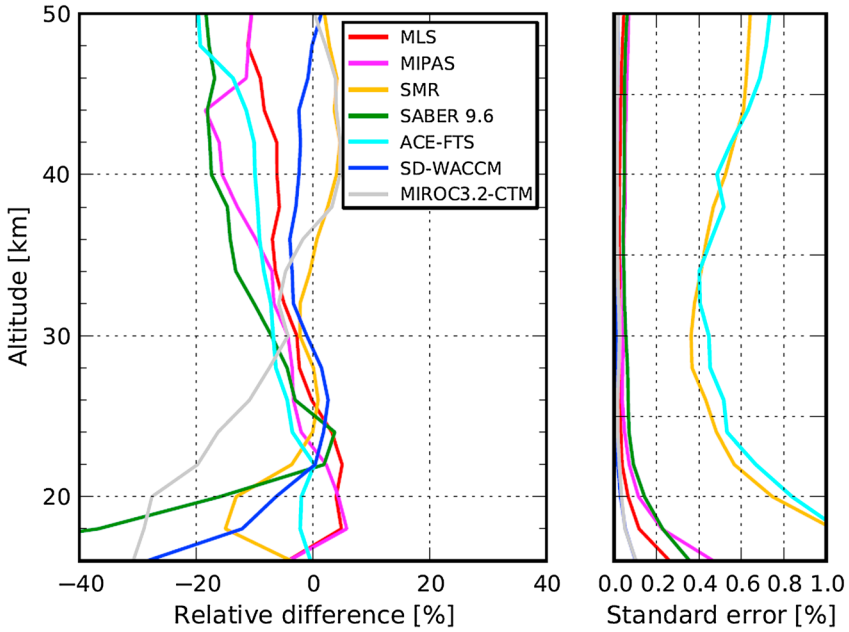

Figure 9. Average relative differences between SMILES and other data sets over all latitude bands and their standard errors. Relative differences are calculated by using equation (5); correlatives are subtracted from SMILES.

determination that cause the systematic error of SMILES ozone, and nonlinearity correction and pressure broadening parameters are considered the main causes. Based on the results in this subsection 5.1, we can conclude that the lower limit for scientific use of the SMILES ozone data is an altitude of 16 km, but caution is required below 22 km, particularly in the equatorial latitudes because of some positive biases that can reach 5%–8%.

5.2. Comparisons in the Mesosphere

[43] Ozone concentration shows such a strong diurnal variation in the mesosphere [e.g., *Huang et al.*, 2010] that we separated daytime and nighttime profiles in solar zenith angle (SZA) to be 0° "≤ SZA ≤ 60° and 120° ≤ SZA ≤ 180°, respectively. Figure 10 shows vertical profile comparisons with MLS as shown in Figure 3, but with daytime mesospheric ozone as red lines and nighttime as blue lines. The agreement for the daytime is within 14% up to around 67 km, but the differences increase considerably above 70 km. The agreement for the nighttime is also mostly good (within 14%) up to 70 km, but again deteriorates above 70 km. In general, at higher altitudes we see large variability, because the precision of the ozone profile decreases owing to the lower ozone abundance. In Figure 10 we found that the standard deviation gradually becomes larger as the altitude increases, but this is mainly caused by variations in the precision of the MLS ozone [*Froidevaux et al.*, 2008]. The precision of the SMILES ozone is better, as is evident from the comparisons with SD-WACCM, which will be shown later.

[44] Figure 11 is the same as Figure 10 except for SABER 9.6 observations. The other SABER ozone band (SABER 1.27) can only be used for daytime measurements. Here we present comparison results using SABER 9.6 for both daytime and nighttime, and some results from SABER 1.27 will be shown later in Figure 14. Since no northern high latitude data satisfy the coincidence criteria during daytime, only nighttime comparisons are plotted in the uppermost figure. The agreement for daytime SABER 9.6 is within 30% up to 54 km, while the agreement for nighttime stays around 30% up to 73 km. Both daytime and nighttime values of SABER 9.6 ozone are large compared with those of the SMILES. The positive bias of the SABER ozone data is a known problem [*Rong et al.*, 2009], and the better agreement with the 1.27 μm band is supported by results from a comparison between the two SABER bands and the HAMMONIA model [*Dikty et al.*, 2010, and references therein]. This will be further examined in Figure 14.

[45] Figure 12 is the same as Figure 10 except for SD-WACCM. Daytime agreement is good, within 7% below 56 km and still within 30% up to 73 km, while the agreement

Figure 8. Scatter plots at three representative altitudes for SMILES versus reference ozone (from top to bottom): MLS, MIPAS, SMR, SABER 9.6, ACE-FTS, SD-WACCM, and MIROC3.2-CTM. Measurement pairs are represented as colored points, and the average values in each 10° latitude bin are shown by large symbols with a black border with the error bars denoting standard deviation. Red indicates low latitudes and blue high latitudes. Note that the standard deviation includes both the measurement uncertainty and atmospheric variability for about 6 months from October 2009 to April 2010. The black solid lines are the best-fit linear equations for the average values. The gradient, intercept, and correlation derived from the best-fit line are indicated on the top left of each figure. Note also that the coincident CTM data have been reduced by a factor of 10 because of the quantity of data.

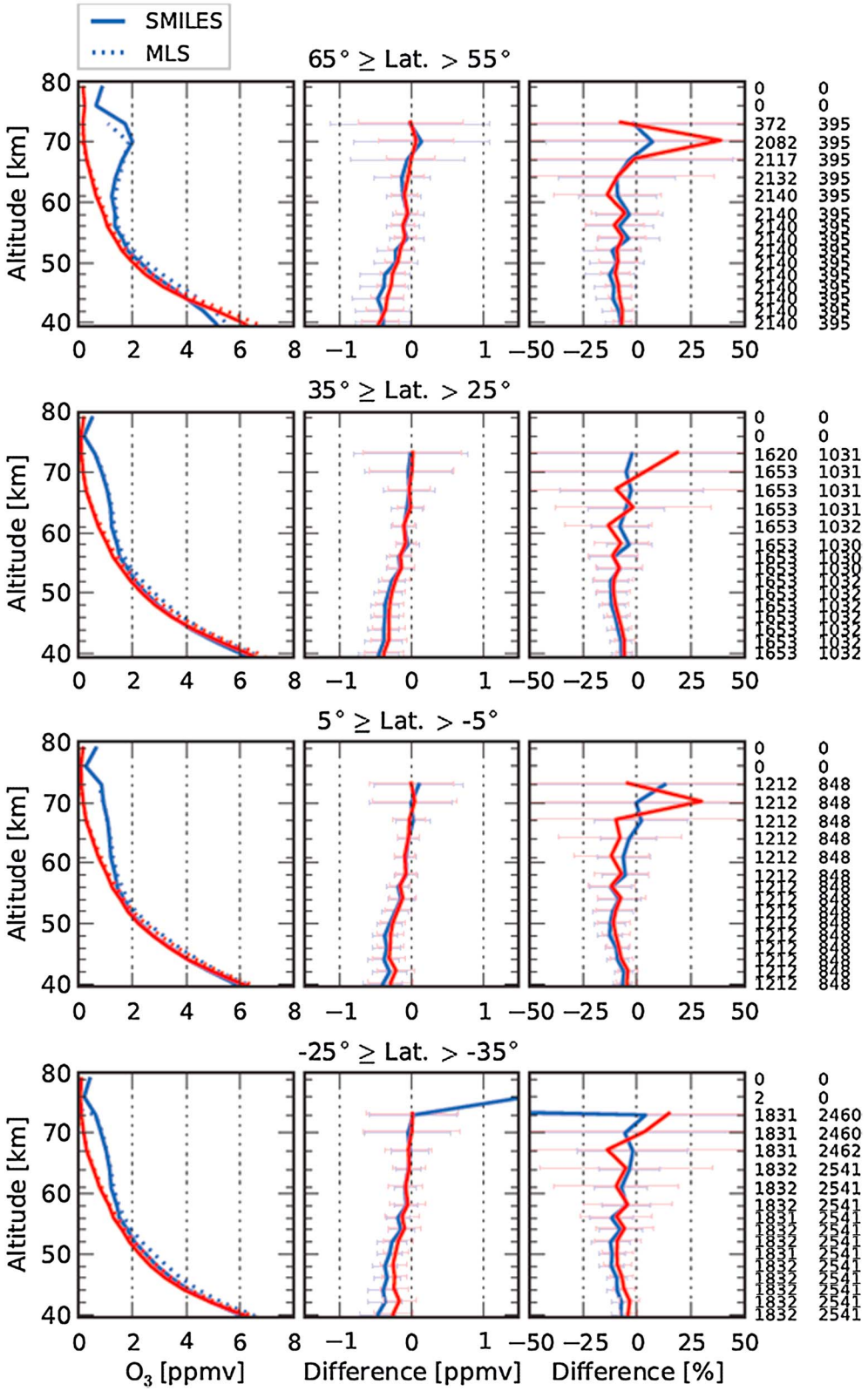

Figure 10. SMILES-MLS coincidences in the mesosphere at four representative latitudes: (from top to bottom) 55°N–65°N, 25°N–35°N, 5°S–5°N, and 35°S–25°S, (left) average values, (middle) average differences, and (right) average relative differences. The red and blue lines are the comparisons of daytime and nighttime ozone, and the averaged profiles of SMILES and MLS are represented as solid and dashed lines, respectively. The error bars of the differences and the relative differences are ±1 standard deviations. The numbers shown on each SMILES altitude level on the right axes are the profile numbers of daytime (right) and nighttime (left) for the statistics.

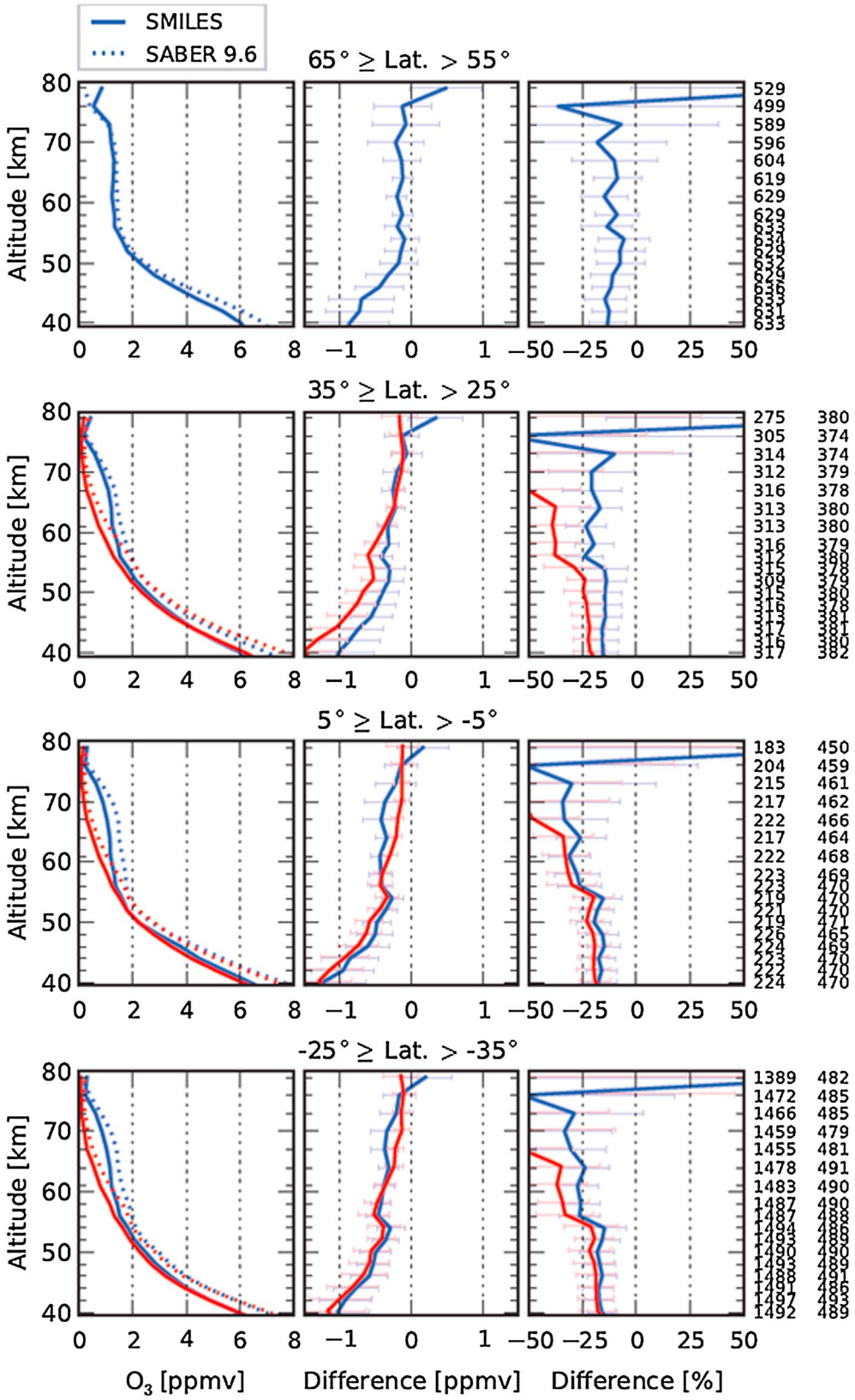

Figure 11. Same as for Figure 10 except for comparisons between SMILES and SABER 9.6.

at nighttime is within 7% (9%) up to 58 (70) km at the high (mid and low) latitudes. The quality of the SMILES ozone profiles could be estimated from the number of available ozone profiles and the standard deviations in the comparisons with SD-WACCM, because model results do not include measurement uncertainty and represent ideal distributions. The number of ozone profiles decreases and the standard deviations become dramatically large, above 73 km. The

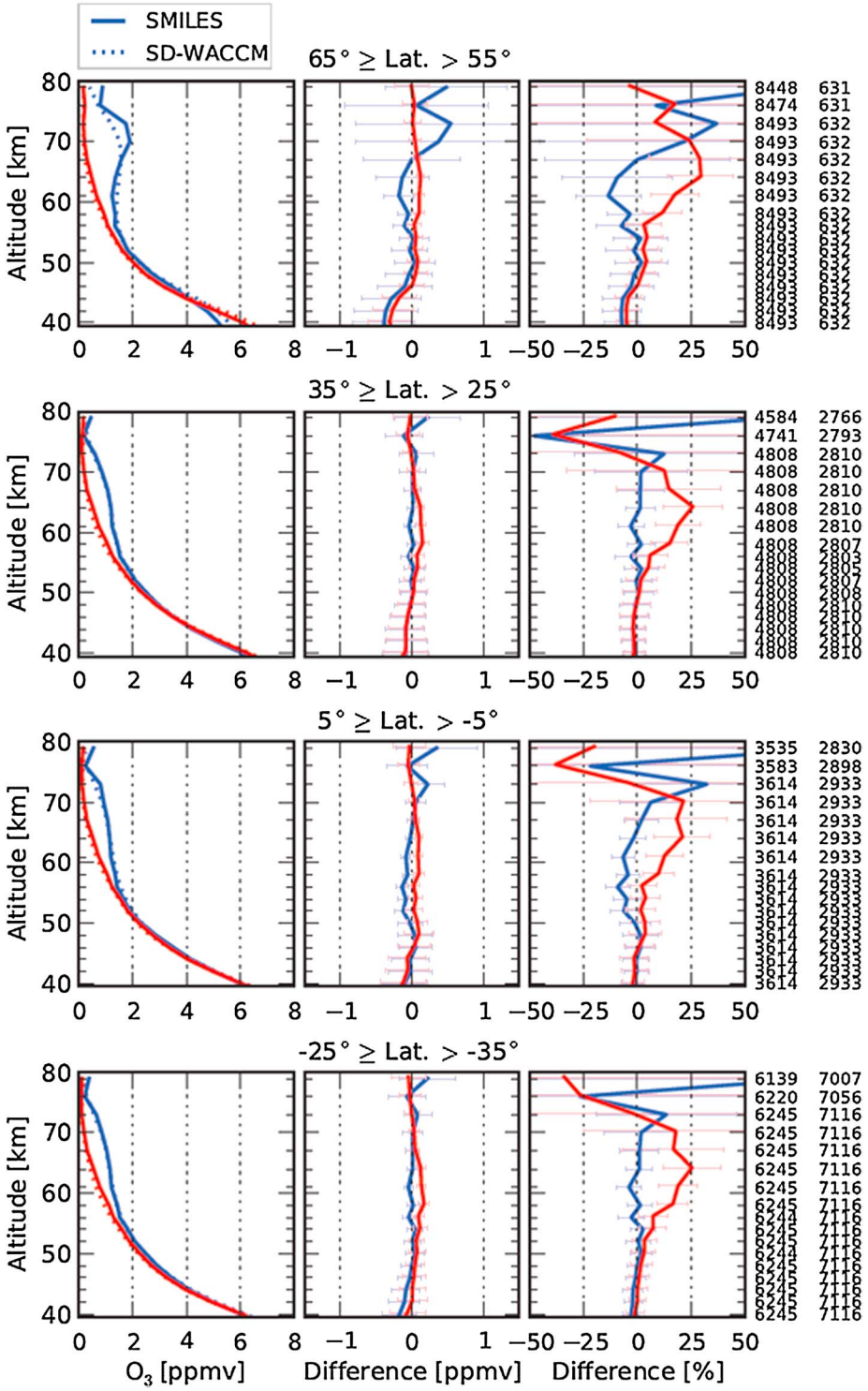

Figure 12. Same as for Figure 10 except for comparisons between SMILES and SD-WACCM.

error ratio also becomes large, above 73 km, as we saw in Figure 1. Therefore, we recommend an altitude of 73 km as the upper limit for scientific use for this version of the SMILES ozone data. However, we are now preparing for the next L2 product (v2.2) in which a new inversion model is employed, using the Tikhonov regularization method [*Eriksson*, 2000], the retrieval altitude range is extended up to 90 km, and several important updates are included. We have confirmed that the useful altitude range of the next version extends to higher altitudes than the current version.

[46] Finally, we investigate ozone variations in the tropics (10°N–10°S) as a function of local time. To extract diurnal variations, we followed a process similar to that originally proposed by *Sakazaki et al*. [2013] in which diurnal ozone variations are investigated using the SMILES data: First, we averaged the data over longitude in the equatorial latitude

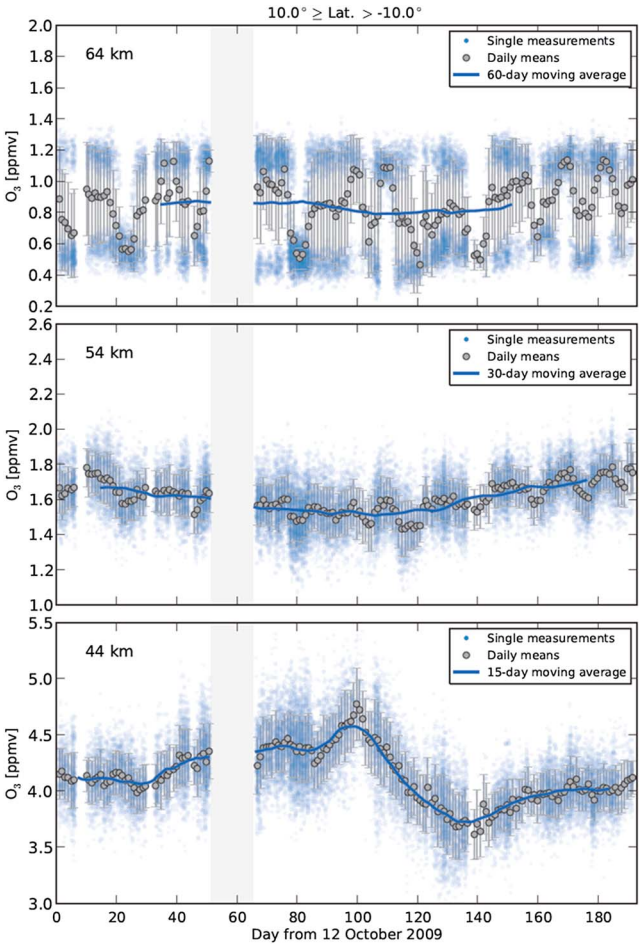

Figure 13. Time series of SMILES measurements at three representative altitudes. The individual measurements are shown in semitransparent blue. The daily means and their standard deviations are shown as large grey dots with black borders and grey error bars, respectively. The solid blue lines are moving averages.

band (10°S–10°N) each day and the seasonal time scale components were derived from the SMILES data at altitude levels of 44, 54, and 64 km, using moving averages. The deviation from the mean of the seasonal components were subtracted from the original time series of each coincident data set, and we then binned the data within 1 hour LT and averaged each bin. Since the SMILES observations are not continuous in time because of, for example, field-of-view interference with the ISS solar paddle [*Kikuchi et al.*, 2010a], we can easily lose data that might allow us to extract the diurnal variation. To derive the seasonal variations, we must be careful about the relative amplitude of the seasonal and diurnal variations; the seasonal variation is dominant in the stratosphere but the situation reverses in the mesosphere. Therefore, we adjusted the width of the moving average and subtracted 15 day, 30 day, and 60 day moving averages from the coincident data at three altitudes of 44, 54, and 64 km, respectively (see also Figure 13).

[47] Figure 14 shows plots of diurnal variation of ozone at three representative altitudes: 44, 54, and 64 km; some of these altitudes are overlapped as in *Sakazaki et al.* [2013]. The SMILES and SABER measurements can provide data over a range of LT, while other satellite data are limited to fixed LT because of a sun-synchronous orbit (see also Table 3). Note that in daytime, both SABER 9.6 and 1.27 provide data at the coincidence locations, but at nighttime only SABER 9.6 data are available for limited local times because of the limited measurements coincident with SMILES. A detailed explanation of the underlying mechanism for the diurnal ozone variation in the stratosphere and the mesosphere has been described in *Sakazaki et al.* [2013]. In this study, we will mainly show the comparison results.

[48] At 44 km, the inter-satellite comparisons show that SMILES agrees within 1 σ with MLS, SMR, and the limited LTs of SABER 1.27, but the MIPAS and SABER 9.6 measurements show rather large values. As we expand the range of ozone mixing ratios to include most of all available data, the diurnal variation becomes unclear. However, as shown in *Sakazaki et al.* [2013], it is captured well in the SMILES and CTM data, with a peak-to-peak amplitude about 0.2 ppmv.

[49] At 54 km, the agreement within 1 σ remains for MLS, SMR, and the limited LTs of SABER 1.27; SABER 9.6

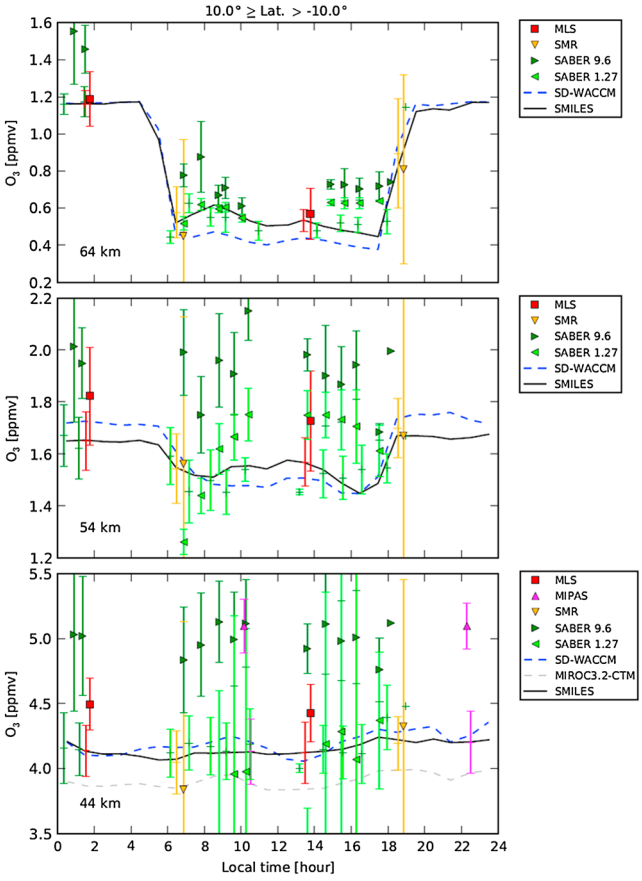

Figure 14. Diurnal variation at equatorial latitudes for three representative altitudes. The solid and dashed lines are derived from SMILES and CTMs at SMILES observation locations and times, respectively. Symbols (see legend) are used for the averaged satellite data with the coincident SMILES data as crosses of the same color. Error bars denote standard deviations calculated by separating both seasonal and diurnal variations. The colors of the lines are the same as those in Figure 9.

measurements still show rather large values. SMILES and SD-WACCM track each other well, except that the amplitudes of SD-WACCM are around 1.5–2.0 times larger than those in SMILES. This feature is described in detail in *Sakazaki et al*. [2013]. They concluded that the lower limit of the dominance of the nighttime enhancement of ozone is located at 50 km in the SMILES data but at 46 km in the CTMs, resulting in smaller amplitudes in the SMILES data than in the CTMs at 50–60 km.

[50] At 64 km, the diurnal variation is well represented by SMILES and SD-WACCM; the agreement is particularly good at nighttime, before 06:00 and after 18:00 LT. Also, the MLS and SMR measurements agree well. The difference between SABER 1.27 and 9.6 during the daytime becomes small and almost within the error bars, although the values are still somewhat higher than SMILES even for the nighttime SABER 9.6.

6. Summary

[51] SMILES observed global ozone in the middle atmosphere from 12 October 2009 to 21 April 2010. We have presented validation studies of the SMILES v2.1 ozone product based on a comparison with satellite observations and CTMs. The comparisons of stratospheric ozone show good agreement within 10%. In the mesosphere, the agreement is also good and better than 30% even at a high altitude of 73 km. In addition, the LT-independent SMILES measurements capture the diurnal variability very well. The recommended altitude range for scientific use is from 16 to 73 km. However, the following features should be kept in mind for the use of the SMILES ozone data: (i) data quality is poor below 18 km, especially at lower latitudes; (ii) there is a positive bias of smaller than 8% below ~24 km in the equatorial latitudes; and (iii) values tend to be lower than correlative satellite data from ~26 km, and increasingly so at the higher altitudes to 50 km, as seen in comparison with MLS and more clearly in comparison with MIPAS, SABER 9.6, and ACE-FTS.

[52] SMILES has produced a new and extensive data set relating to the Earth's atmospheric composition. The high sensitivity and LT-independent measurements of SMILES provide an opportunity to investigate atmospheric phenomena in the stratosphere and the mesosphere in unprecedented detail.

[53] **Acknowledgments.** This study was supported in part by the Japanese Ministry of Education, Culture, Sports, Science and Technology (MEXT) through a Grant-in-Aid for Scientific Research (22310010), the ISS Science Project Office of ISAS/JAXA, and the Global Environment Research Fund of the Japanese Ministry of the Environment (A-0903). SMILES data obtained from Data Archives and Transmission System (DARTS), provided by Center for Science-satellite Operation and Data Archive (C-SODA) at ISAS/JAXA. The Atmospheric Chemistry Experiment (ACE), also known as SCISAT, is a Canadian-led mission mainly supported by the Canadian Space Agency and the Natural Sciences and Engineering Research Council of Canada. Computations for MIROC3.2-CTM were made on the NEC SX-8R computers at the Center for Global Environmental Research (CGER), National Institute for Environmental Studies (NIES). The authors also thank the MIROC model development group at AORI in the University of Tokyo, JAMSTEC, and NIES, and K. Sudo in Nagoya University. The National Center for Atmospheric Research (NCAR) is sponsored by U.S. National Science Foundation.

References

Akiyoshi, H., L. B. Zhou, Y. Yamashita, K. Sakamoto, M. Yoshiki, T. Nagashima, M. Takahashi, J. Kurokawa, M. Takigawa, and T. Imamura (2009), A CCM simulation of the breakup of the Antarctic polar vortex in the years 1980–2004 under the CCMVal scenarios, *J. Geophys. Res.*, *114*, D03103, doi:10.1029/2007JD009261.

Akiyoshi H., Yamashita Y., K. Sakamoto, L. B. Zhou, and T. Imamura (2010), Recovery of stratospheric ozone in calculations by the Center for Climate System Research/National Institute for Environmental Studies chemistry-climate model under the CCMVal-REF2 scenario and a no-climate-change run, *J. Geophys. Res.*, *115*, D19301, doi:10.1029/2009JD012683.

Austin, J., et al. (2010a), Decline and recovery of total column ozone using a multimodel time series analysis, *J. Geophys. Res.*, *115*, D00M10, doi:10.1029/2010JD013857.

Austin, J., et al. (2010b), Chemistry-climate model simulations of spring Antarctic ozone, *J. Geophys. Res.*, *115*, D00M11, doi:10.1029/2009JD013577.

Bernath, P. F. (2006), Atmospheric Chemistry Experiment (ACE): Analytical chemistry from orbit, *Trends Anal. Chem.*, *25*(7), 647–654.

Bernath, P. F., et al. (2005), Atmospheric Chemistry Experiment (ACE): Mission overview, *Geophys. Res. Lett.*, *32*, L15S01, doi:10.1029/2005GL022386.

Boone, C. D., R. Nassar, K. A. Walker, Y. Rochon, S. D. McLeod, C. P. Rinsland, and P. F. Bernath (2005), Retrievals for the atmospheric chemistry experiment Fourier-transform spectrometer, *Appl. Opt.*, *44*, 7218–7231.

Butchart N., et al. (2011), Multimodel climate and variability of the stratosphere, *J. Geophys. Res.*, *116*, D05102, doi:10.1029/2010JD014995.

Cortesi, U., et al. (2007), Geophysical validation of MIPAS-ENVISAT operational ozone data. *Atmos. Chem. Phys.*, *7*, 4807–4867.

Dikty, S., H. Schmidt, M. Weber, C. von Savigny, and M. G. Mlynczak (2010), Daytime ozone and temperature variations in the mesosphere: A comparison between SABER observations and HAMMONIA model, *Atmos. Chem. Phys.*, *10*, 8331–8339, doi:10.5194/acp-10-8331-2010.

Dupuy, E., et al. (2009), Validation of ozone measurements from the Atmospheric Chemistry Experiment (ACE), *Atmos. Chem. Phys.*, *9*, 287–343, doi:10.5194/acp-9-287-2009.

Emmons, L. K., et al. (2010), Description and evaluation of the Model for Ozone and Related chemical Tracers, version 4 (MOZART-4), *Geosci Model Dev.*, *3*, 43–67, doi:10.5194/gmd-3-43-2010.

Eriksson, P. (2000), Analysis and comparison of two linear regularization methods for passive atmospheric observations, *J. Geophys. Res.*, *105* (D14), 18,157–18,167, doi:10.1029/2000JD900172.

Eyring, V., et al. (2007), Multimodel projections of stratospheric ozone in the 21st century, *J. Geophys. Res.*, *112*, D16303, doi:10.1029/2006JD008332.

Eyring, V., et al. (2010), Multi-model assessment of stratospheric ozone return dates and ozone recovery in CCMVal-2 models, *Atmos. Chem. Phys.*, *10*, 9451–9472, doi:10.5194/acp-10-9451-2010, www.atmos-chem-phys.net/10/9451/2010/.

Fischer, H., et al. (2008), MIPAS: An instrument for atmospheric and climate research, *Atmos. Chem. Phys.*, *8*, 2151–2188, doi:10.5194/acp-8-2151-2008.

Frisk, U., et al. (2003), The Odin satellite - I. Radiometer design and test, *A&A*, *402*, L27–L34, doi:10.1051/0004-6361:20030335.

Froidevaux, L., et al. (2008), Validation of Aura Microwave Limb Sounder stratospheric ozone measurements, *J. Geophys. Res.*, *113*, D15S20, doi:10.1029/2007JD008771.

Garcia, R. R., D. R. Marsh, D. E. Kinnison, B. A. Boville, and F. Sassi (2007), Simulations of secular trends in the middle atmosphere, 1950–2003, *J. Geophys. Res.*, *112*, D09301, doi:10.1029/2006JD007485.

Hoffmann, C. G., D. E. Kinnison, R. R. Garcia, M. Palm, J. Notholt, U. Raffalski, and G. Hochschild (2012), CO at 40–80 km above Kiruna observed by the ground-based microwave radiometer KIMRA and simulated by the Whole Atmosphere Community Climate Model, *Atmos. Chem. Phys.*, *12*, 559–587, doi:10.5194/acpd-12-559-2012.

Huang, F. T., H. G. Mayr, J. M. Russell, III, and M. G. Mlynczak (2010), Ozone diurnal variations in the stratosphere and lower mesosphere, based on measurements from SABER on TIMED, *J. Geophys. Res.*, *115*, D24308, doi:10.1029/2010JD014484.

Jégou, E., et al. (2008), Technical Note: Validation of Odin/SMR limb observations of ozone, comparisons with OSIRIS, POAM III, ground-based and balloon-borne instruments, *Atmos. Chem. Phys.*, *8*, 3385–3409.

JEM/SMILES L2 Products Guide for v2.1 (2012), Available at http://darts.isas.jaxa.jp/iss/smiles/docs/L2dataGuide_2-1.pdf.

Kikuchi K., et al. (2010a), Overview and early results of the Superconducting Submillimeter-Wave Limb-Emission Sounder (SMILES), *J. Geophys. Res.*, *115*, D23306, doi:10.1029/2010JD014379.

Kikuchi K., T. Nishibori, S. Ochiai, T. Manabe, H. Ozeki, R. Sato, T. Sano, Y. Irimajiri, and M. Shiotani (2010b), Instrument Overview and Operation of JEM/SMILES, Proc. International Archives of the Photogrammetry, Remote Sensing and Spatial Information Science (ISPRS) Technical Comission VIII Symposium, p. 100.

Kinnison, D. E., et al. (2007), Sensitivity of chemical tracers to meteorological parameters in the MOZART-3 chemical transport model, *J. Geophys. Res.*, *112*, D20302, doi:10.1029/2006JD007879.

Kunz, A., L. L. Pan, P. Konopka, D. E. Kinnison, and S. Tilmes (2011), Chemical and dynamical discontinuity at the extratropical tropopause based on START08 and WACCM analyses, *J. Geophys. Res.*, *116*, D24302, doi:10.1029/2011JD016686.

Lamarque, J.-F., et al. (2012), CAM-chem: description and evaluation of interactive atmospheric chemistry in CESM, *Geosci. Model Dev.*, *5*, 369–411, doi:10.5194/gmd-5-369-2012.

Levenberg K. A. (1944), Method for the solution of certain problems in least squares, *QJ Appl. Math.*, *2*, 164–8.

Lin, S.–. J. (2004), A "vertically Lagrangian" finite-volume dynamical core for global models, *Mon. Wea. Rev.*, *132*, 2293–2307.

Livesey, N. J., W. Van Snyder, W. G. Read, and P. A. Wagner (2006), Retrieval algorithms for the EOS Microwave Limb Sounder (MLS), *IEEE Trans. Geosci. Remote Sens.*, *44*(5), 1144–1155.

Marquardt D. W. (1963) An algorithm for the least-squares estimation of nonlinear parameters, *SIAM J. Appl. Math.*, *11*(2), 431–41.

Mieruch, S., et al. (2012), Global and long-term comparison of SCIAMACHY limb ozone profiles with correlative satellite data (2002–2008), *Atmos. Meas. Tech.*, *5*, 771–788, doi:10.5194/amt-5-771–2012.

Mitsuda, C., et al. (2011), Current status of level 2 product of Superconducting Submillimeter-Wave Limb-Emission Sounder (SMILES), *Proc. SPIE*, *8176*, 81760M.

Mlynczak, M. G., B. T. Marshall, F. J. Martin-Torres, J. M. Russell III, R. E. Thompson, E. E. Remsberg, and L. L. Gordley (2007), Sounding of the Atmosphere using Broadband Emission Radiometry observations of daytime mesospheric $O_2(^1\Delta)$ 1.27 μm emission and derivation of ozone, atomic oxygen, and solar and chemical energy deposition rates, *J. Geophys. Res.*, *112*, D15306, doi:10.1029/2006JD008355.

Moritz, H. (2000), Geodetic reference system 1980, *J. Geodesy*, *74*, 128–162, 10.1007/s001900050278.

Murtagh, D., et al. (2002), *Can. J. Phys.*, *80*, 309–319.

Narasaki, K., S. Tsunematsu, S. Yajima, A. Okabayashi, J. Inatani, K. Kikuchi, R. Satoh, T. Manabe, and M. Seta (2004), Development of cryogenic system for SMILES, *AIP Conf. Proc.*, *710*(1), 1785–1796.

Ochiai, S., et al. (2010), Performance of JEM/SMILES in orbit. *21st Int'l Symp on Space Terahertz Technol.*, S8.1, (Oxford, UK), March 2010.

Ochiai, S., K. Kikuchi, T. Nishibori, T. Manabe (2012), Gain nonlinearity calibration of submillimeter radiometer for JEM/SMILES, *IEEE J. Sel. Topics Appl. Earth Observ. Remote Sens.*, *5*(3), 962–969, doi:10.1109/JSTARS.2012.2193559.

Oman, L. D., et al. (2010), Multimodel assessment of the factors driving stratospheric ozone evolution over the 21st century, *J. Geophys. Res.*, *115*, D24306, doi:10.1029/2010JD014362.

Ozeki, H., Y. Kasai, S. Ochiai, S. Tsujimaru, J. Inatani, H. Masuko, C. Takahashi, L. Mazuray, and C. Rosolen (2000), Submillimeter wave spectroscopy performance of JEM/SMILES, SPIE's Second International Asia-Pacific Symposium on Remote Sensing of the Atmosphere, Environment and Space, Sendai, Japan, Oct. 9–12, 2000, *Proc. of SPIE*, 4152, pp. 255–262.

Pickett, H. M., R. L. Poynter, and E. A. Cohen (1992), Submillimeter, millimeter, and microwave spectral line catalogue, Technical Report JPL Publication 80–23, Rev.3, JPL.

Randel, W. J., M. Park, L. Emmons, D. Kinnison, P. Bernath, K. A. Walker, C. Boone, and H. Pumphrey (2010), Asian monsoon transport to the stratosphere, *Science*, *328*(5978), 611–613, doi:10.1126/science.1182274.

Rienecker, M. M., et al. (2008), The GEOS-5 data assimilation system—Documentation of versions 5.0.1, 5.1.0, and 5.2.0, NASA Technical Report Series on Global Modeling and Data Assimilation, V27, NASA/TM-2008-104606.

Rodgers, C. D. (1976), Retrieval of atmospheric temperature and composition from remote measurements of thermal radiation, *Rev. Geophys.*, *14*(4), 609–624.

Rodgers, C. D. (1990), Characterization and error analysis of profiles retrieved from remote sounding measurements, *J. Geophys. Res.*, *95*(D5), 5587–5595.

Rodgers, C. D. (2000), *Inverse Methods for Atmospheric Sounding: Theory and Practice (Ser. on Atmos., Oceanic, and Planet. Phys)*., vol. *2*, World Scientific, Singapore.

Rong, P. P., J. M. Russell III, M. G. Mlynczak, E. E. Remsberg, B. T. Marshall, L. L. Gordley, and M. López-Puertas (2009), Validation of thermosphere ionosphere mesosphere energetics and dynamics/sounding of the atmosphere using broadband emission radiometry (TIMED/SABER) v1.07 Ozone at 9.6 mm in altitude range 15–70 km, *J. Geophys. Res.*, *114*, D04306, doi:10.1029/2008JD010073.

Rothman, L. S., et al. (2009), The HITRAN 2008 molecular spectroscopic database, *J. Quant. Spectrosc. Radiat. Trans.*, *110*, 533–572, doi:10.1016/j.jqsrt.2009.02.013.

Russell, J. M., III, M. G. Mlynczak, L. L. Gordley, J. J. Larry Tansock, and R. Esplin (1999), Overview of the SABER experiment and preliminary calibration results, *Proc. SPIE Int. Soc. Opt. Eng.*, *3756*, 277–288.

Sakazaki T., et al. (2013), Diurnal ozone variations in the stratosphere revealed in observations from the Superconducting Submillimeter-Wave Limb-Emission Sounder (SMILES) onboard the International Space Station (ISS), *J. Geophys. Res.*, *118*, doi:10.1002/jgrd.50220.

Sander, S. P., et al. (2006), Chemical kinetics and photochemical data for Use in atmospheric studies—Evaluation number 15, *JPL Publication* 06–2.

Schoeberl, M. R., et al. (2006), Overview of the EOS Aura mission, *IEEE Trans. Geosci. Remote Sens.*, *44*, 1066.1074.

Smith, A. K., et al. (2013), Satellite observations of ozone in the upper mesosphere, *J. Geophys. Res.*, doi:10.1002/jgrd.50445.

SPARC CCMVal (2010), *SPARC Report on the Evaluation of Chemistry-Climate Models*, edited by V. Eyring, T. G. Shepherd, D. W. Waugh, SPARC Report No.5, WCRP-132, WMO/TD-No.1526.

Steck, T., et al. (2007), Bias determination and precision validation of ozone profiles from MIPAS-Envisat retrieved with the IMK-IAA processor, *Atmos. Chem. Phys.*, *7*, 3639–3662, doi:10.5194/acp-7-3639-2007.

Stiller, G. P., et al. (2012), Validation of MIPAS IMK/IAA temperature, water vapor, and ozone profiles with MOHAVE-2009 campaign measurements, *Atmos. Meas. Tech.*, *5*, 289–320, doi:10.5194/amt-5-289-2012.

Strahan, S. E., et al. (2011), Using transport diagnostics to understand chemistry climate model ozone simulations, *J. Geophys. Res.*, *116*, D17302, doi:10.1029/2010JD015360.

Takahashi, C., S. Ochiai, and M. Suzuki (2010), Operational retrieval algorithms for JEM/SMILES level 2 data processing system, *J. Quant. Spectrosc. Radiat. Transfer*, *111*, 160–173.

Takahashi, C., et al. (2011), Capability for ozone high-precision retrieval on JEM/SMILES observation, *Adv. Space Res.*, *48*, 1076–1085.

Urban, J., et al. (2004), The northern hemisphere stratospheric vortex during the 2002–03 winter: Subsidence, chlorine activation and ozone loss observed by the Odin Sub-Millimeter Radiometer, *Geophys. Res. Lett.*, *31*, L07103, doi:10.1029/2003GL019089.

Urban, J., et al. (2005), Odin/SMR limb observations of stratospheric trace 5 gases: Level 2 processing of ClO, N2O, HNO3, and O3, *J. Geophys. Res.*, *110*, D14307, doi:10.1029/2004JD005741.

Verronen, P. T., et al. (2005), A comparison of night-time GOMOS and MIPAS ozone profiles in the stratosphere and mesosphere, *Adv. Space Res.*, *36*, S.958–66, doi:10.1016/j.asr.2005.04.073.

von Clarmann, T., et al. (2003), Retrieval of temperature and tangent altitude pointing from limb emission spectra recorded from space by the Michelson Interferometer for Passive Atmospheric Sounding (MIPAS), *J. Geophys. Res.*, *108*(D23), 4736, doi:10.1029/2003JD003602.

von Clarmann, T., et al. (2009), Retrieval of temperature, H_2O, O_3, HNO_3, CH_4, N_2O, $ClONO_2$ and ClO from MIPAS reduced resolution nominal mode limb emission measurements, *Atmos. Meas. Tech.*, *2*, 159–175, doi:10.5194/amt-2-159-2009.

Waters, J. W., et al. (2006), The Earth Observing System Microwave Limb Sounder (EOS MLS) on the Aura satellite, *IEEE Trans. Geosci. Remote Sens.*, *44*(5), 1175–1092.

Waymark, C., K. Walker, C. Boone, E. Dupuy, and P. Bernath (2011), Validation of the ACE-FTS version 3.0 Dataset against other satellite instrument datasets, in Fourier transform spectroscopy, OSA Technical Digest (CD) (Optical Society of America, 2011), paper FMB4.

WMO (World Meteorological Organization) (2007), Scientific assessment of ozone depletion: 2006, Global Ozone Research and Monitoring Project-Report No. 50, Geneva, Switzerland.

Zhang, X., J. M. Forbes, and M. E. Hagan (2010a), Longitudinal variation of tides in the MLT region: 1. Tides driven by tropospheric net radiative heating, *J. Geophys. Res.*, *115*, A06316, doi:10.1029/2009JA014897.

Zhang, X., J. M. Forbes, and M. E. Hagan (2010b), Longitudinal variation of tides in the MLT region: Part 2, Relative effects of solar radiative and latent heating, *J. Geophys. Res.*, A06317, doi:10.1029/2009JA014898.